The dual function monoclonal antibodies VIR-7831 and VIR-7832 demonstrate potent in vitro and in vivo activity against SARS-CoV-2

Andrea L. Cathcart[1], Colin Havenar-Daughton[1], Florian A. Lempp[1], Daphne Ma[1], Michael A. Schmid[2], Maria L. Agostini[1], Barbara Guarino[2], Julia Di iulio[1], Laura E. Rosen[1], Heather Tucker[1], Joshua Dillen[1], Sambhavi Subramanian[1], Barbara Sloan[1], Siro Bianchi[2], Dora Pinto[2], Christian Saliba[2], Jason A Wojcechowskyj[1], Julia Noack[1], Jiayi Zhou[1], Hannah Kaiser[1], Arthur Chase[1], Martin Montiel-Ruiz[1], Exequiel Dellota Jr.[1], Arnold Park[1], Roberto Spreafico[1], Anna Sahakyan[1], Elvin J. Lauron[1], Nadine Czudnochowski[1], Elisabetta Cameroni[1], Sarah Ledoux[1], Adam Werts[3], Christophe Colas[1], Leah Soriaga[1], Amalio Telenti[1], Lisa A. Purcell[1], Seungmin Hwang[1], Gyorgy Snell[1], Herbert W. Virgin[1], Davide Corti[2], Christy M. Hebner[1*]

[1]Vir Biotechnology, San Francisco, California 94158, USA

[2]Humabs Biomed SA, a subsidiary of Vir Biotechnology, 6500 Bellinzona, Switzerland

[3]Lovelace Biomedical, Albuquerque, New Mexico 87108, USA

*corresponding author: chebner@vir.bio

ABSTRACT

VIR-7831 and VIR-7832 are dual action monoclonal antibodies (mAbs) targeting the spike glycoprotein of severe acute respiratory syndrome coronavirus 2 (SARS-CoV-2). VIR-7831 and VIR-7832 were derived from a parent antibody (S309) isolated from memory B cells of a 2003 severe acute respiratory syndrome coronavirus (SARS-CoV) survivor. Both mAbs contain an "LS" mutation in the Fc region to prolong serum half-life and potentially enhance distribution to the respiratory mucosa. In addition, VIR-7832 encodes an Fc GAALIE mutation that has been shown previously to evoke CD8+ T-cells in the context of an in vivo viral respiratory infection. VIR-7831 and VIR-7832 potently neutralize wild-type and variant authentic virus in vitro as well as variant pseudotyped viruses. In addition, they retain activity against monoclonal antibody resistance mutations conferring reduced susceptibility to currently authorized mAbs. The VIR-7831/VIR-7832 epitope does not overlap with mutational sites in current variants of concern and continues to be highly conserved among circulating sequences consistent with the high barrier to resistance observed in vitro. Furthermore, both mAbs can recruit effector mechanisms in vitro that may contribute to clinical efficacy via elimination of infected host cells. In vitro studies with these mAbs demonstrated no enhancement of infection. In a Syrian Golden hamster proof-of concept wildtype SARS-CoV-2 infection model, animals treated with VIR-7831 had less weight loss, and significantly decreased total viral load and infectious virus levels in the lung compared to a control mAb. Taken together, these data indicate that VIR-7831 and VIR-7832 are promising new agents in the fight against COVID-19.

INTRODUCTION

The coronavirus disease (COVID-19) pandemic caused by severe acute respiratory syndrome coronavirus 2 (SARS-CoV-2) has resulted in more than 191 million confirmed cases and over 4 million deaths

47 worldwide[1]. SARS-CoV-2 infection results in a broad range of disease severity[2]. Infection fatality rates
48 increase significantly with age, with 28.3% of COVID-19 patients over the age of 85 succumbing to
49 disease[2]. However, even in mild-to-moderate COVID-19 patients, significant post-infection sequelae can
50 affect overall health and cause long-term disability[3]. While multiple SARS-CoV-2 vaccines are now
51 authorized for use, issues of supply, vaccine hesitancy and emergence of variants may prevent rapid
52 attainment of herd immunity[4–9]. In addition, there may be individuals who remain at risk despite
53 vaccination due to disease or underlying immunodeficiency. Thus, additional interventions and potential
54 prophylactic agents are needed to reduce morbidity and mortality due to COVID-19.

55 Several monoclonal antibodies (mAbs) targeting the SARS-CoV-2 spike protein have recently been
56 authorized for use in early treatment of COVID-19 patients[10–13] and clinical data have been reported to
57 show promising results in treatment and prophylactic studies[12–15]. However, rapidly spreading variants
58 exhibit reduced susceptibility in vitro to some currently authorized antibodies that target the receptor
59 binding motif (RBM) of the viral spike (S) glycoprotein [10,11,16,17]. Therefore, mAbs targeting unique S
60 epitopes are needed for use alone or in combination with current agents for the treatment and prevention
61 of COVID-19. Furthermore, in addition to viral neutralization, antibodies possessing potent effector
62 function to aid in the killing of virally infected cells and the elicitation of T cell immunity could
63 significantly assist in halting disease progression[18–20].

64 VIR-7831 and VIR-7832 are dual action mAbs derived from the parent antibody S309 identified from a
65 2003 SARS-CoV survivor[21]. These mAbs target an epitope containing a glycan (at position N343) that is
66 highly conserved within the Sarbecovirus subgenus in a region of the S receptor binding domain (RBD)
67 that does not compete with angiotensin converting enzyme 2 (ACE2) binding[22]. This epitope does not
68 overlap with mutations observed in current variants of concern[10,11,16,17]. The variable region of VIR-7831
69 and VIR-7832 have been engineered for enhanced developability. In addition, both antibodies possess an
70 Fc "LS" mutation that confers extended half-life by binding to the neonatal Fc receptor and potentially
71 enhances distribution to the respiratory mucosa [23–25]. VIR-7832 is identical to VIR-7831 with the

72 exception of the addition of a 3 amino acid GAALIE (G236A, A330L, I332E) modification to the Fc
73 domain[26]. The GAALIE modification has previously been shown in vitro to enhance binding to FcγIIa
74 and FcγIIIa receptors, decrease affinity for FcγIIb compared to typical IgG1 and evoke protective CD8+
75 T-cells in the context of viral respiratory infection in vivo [27,28].

76 Here we characterize the antiviral potential of VIR-7831 and VIR-7832. These mAbs effectively
77 neutralize SARS-CoV-2 live virus in vitro as well as in pseudotyped virus assays against emerging
78 variants of concern and variants that confer resistance to currently authorized mAbs[29]. In addition to the
79 neutralizing capacity, both antibodies demonstrate potent effector function and mediate antibody
80 dependent cellular cytotoxicity (ADCC) and antibody dependent cellular phagocytosis (ADCP) in vitro.
81 Furthermore, resistance selection experiments and epitope conservation analyses indicate the potential for
82 a high barrier to resistance. Data derived from the Syrian golden hamster model demonstrates efficacy in
83 a proof-of-concept in vivo model. Taken together, these data indicate that VIR-7831 and VIR-7832 are
84 promising key components of the arsenal in the fight against COVID-19.

85 **RESULTS**

86 **VIR-7831 and VIR-7832 bind SARS-CoV-2 spike and effectively neutralize live virus in vitro.**
87 Previously published work showed that S309 bound SARS-CoV-2 recombinant and cell surface-
88 associated S and neutralized live virus in vitro[21]. We initiated these studies by repeating and extending
89 these earlier results. To determine the binding activity of VIR-7831 and VIR-7832 to the SARS-CoV-2 S,
90 enzyme-linked immunosorbent assay (ELISA), surface plasmon resonance (SPR) and flow cytometry
91 assays were utilized. VIR-7831 and VIR-7832 bound to recombinant S RBD (amino acids 331-541) with
92 EC_{50} values of 20.40 ng/mL and 14.9 ng/mL, respectively, by ELISA (**Figure 1a**). Using SPR, both
93 antibodies demonstrated potent binding to recombinant S RBD with an equilibrium constant (Kd) of 0.21
94 nM (**Figure 1b**). As antibody recognition of cell surface-bound S could mediate killing of virally infected
95 cells, flow cytometry-based studies using cells transiently transfected with a S-encoding plasmid were

96 used to examine antibody binding to cell surface-expressed S trimer. By this method, both VIR-7831 and
97 VIR-7832 bound efficiently to surface-expressed S (**Figure 1c**).

98 To examine neutralization capacity, VIR-7831 and VIR-7832 were tested in a VeroE6 cell-based live
99 SARS-CoV-2 virus system against the Washington 2019 (wild-type) virus as well as against the Alpha
100 (B.1.1.7), Beta (B.1.351), Gamma (P.1), Delta (B.1.617.2) and Kappa (B.1.617.1) variants.
101 Concentration-dependent viral neutralization of the Washington 2019 strain was observed for both
102 antibodies, with geometric mean $IC_{50/90}$ values of 100.1/186.3 ng/mL and 78.3/253.1 ng/mL, respectively
103 (**Figure 1d**). $IC_{50/90}$ values observed for VIR-7831 and VIR-7832 against the Beta, Gamma, Delta and
104 Kappa variant viruses were similar to those against the wild-type strain. A slight shift in the VIR-
105 7831/VIR-7832 $IC_{50/90}$ compared to wild-type was observed for the Alpha variant. VIR-7831 showed a 3-
106 fold and 4.1-fold shift in IC_{50} and IC_{90}, respectively, against the Alpha variant compared to wild-type
107 while VIR-7832 had a 3.1-fold shift in IC_{50} and 3.7-fold shift in IC_{90} versus wild-type (**Figure 1d, Table**
108 **1)**. As variant evolution is a natural part of SARS-CoV-2 biology and emerging live virus variants are not
109 always readily accessible for testing, a vesicular stomatitis virus (VSV)-based pseudotyped virus system
110 targeting Vero E6 cells was used to examine VIR-7831 and VIR-7832 neutralization against emergent
111 variants (**Table 2**). Fold-changes in VIR-7831 and VIR-7832 IC_{50} values compared to wild-type against
112 pseudotyped virus expressing spike from the Alpha, Beta, Gamma, Delta or Kappa variants were similar
113 to those observed in the authentic virus system. VIR-7831 was tested against an extended panel of
114 pseudotyped viruses incorporating emerging variants as well as all variants deemed as Variants of
115 Concern (VOC) or Variants of Interest (VOI) by the World Health Organization (WHO). VIR-7831
116 retained activity in vitro against all variants tested including all WHO VOCs and VOIs with fold changes
117 in IC_{50}s ranging from 0.4- to 2.3-fold (**Table 2**).

118 **VIR-7831 and VIR-7832 exhibit potent effector function in vitro.** Although direct antiviral
119 mechanisms are crucial to provide protection, Fc-dependent mechanisms mediated by interaction with Fc
120 gamma receptors (FcγRs) on immune cells or with complement, can contribute to overall potency in vivo.

121 The potential for VIR-7831 and VIR-7832 to mediate effector functions were assessed in vitro by
122 measuring binding to FcγRs and C1q and in assays designed to demonstrate antibody-dependent cellular
123 cytotoxicity (ADCC) or antibody-dependent cellular phagocytosis (ADCP)[31–34].

124 Antibody binding to the human activating FcγRIIa (low-affinity R131 and high affinity H131 alleles),
125 FcγRIIIa (low-affinity F158 and high-affinity V158 alleles), and to the inhibitory FcγRIIb were examined
126 using SPR (**Supplemental figure 1a**). VIR-7831 similarly bound both the H131 and R131 alleles of
127 FcγRIIa and binds FcγRIIb. VIR-7831 bound both FcγRIIIa alleles, with reduced binding to the F158
128 allele compared to V158, as is characteristic for human IgG1[35]. Binding of VIR-7831 to C1q was similar
129 to the parental antibody (S309-LS) (**Supplemental figure 1b**). As previously reported for antibodies
130 encoding the GAALIE mutation[26,36], VIR-7832 bound with comparatively higher affinity to activating
131 FcγRIIa and FcγRIIIa than VIR-7831 (**Supplemental figure 1a**). Conversely, VIR-7832 showed reduced
132 affinity for FcγIIb and abrogation of binding to C1q (**Supplemental figure 1b**).

133 The antibodies were also assessed for the ability to activate human FcγRIIa, FcγRIIb or FcγRIIIa, using a
134 Jurkat cell reporter assay[37] (**Figure 2a-d**). S309-GRLR, which contains the effector function-abrogating
135 G236R, L328R mutations was used as a negative control. Cells stably transfected with the SARS-CoV-2
136 spike protein (CHO-CoV-2-Spike) served as target cells. Both VIR-7831 and the parental S309-LS
137 activated signaling of the higher-affinity allele FcγRIIa (H131) but did so less efficiently than the
138 GAALIE-containing antibody VIR-7832 (**Figure 1a**) while VIR-7831, VIR-7832 and S309-LS induced
139 similar low-level activation of the inhibitory receptor FcγRIIb (**Figure 1b**). VIR-7831 demonstrated
140 substantially lower activation of FcγRIIIa F158 versus V158 as expected while VIR-7832 showed
141 increased activation of both alleles of FcγRIIIa (F158 and V158) (**Figures c,d**).

142 To further elucidate the effector function potential of the antibodies, ADCC and ADCP assays were
143 performed using donor PBMCs or NK cells as effector cells and CHO cells stably expressing S (CHO-
144 CoV-2-Spike) as target cells (**Figure 2e-g**). The ability of antibodies to activate NK cell-mediated killing
145 was measured in vitro using two genotyped donors expressing homozygous low-affinity (F/F158) or high-

146 affinity (V/V158) (**Figure 2e-f**). Compared to the parental mAb S309-LS, VIR-7831 had slightly
147 increased capacity to induce NK cell-mediated ADCC when using cells from either F/F158 or V/V158
148 donors. As expected, VIR-7832 induced NK cell-mediated ADCC in cells from donors expressing the
149 low-affinity F/F158 allele of FcγIIIa more efficiently than VIR-7831. These results were confirmed with
150 NK cells from a heterozygous donor (F/V 158).

151 The ability of VIR-7831 and VIR-7832 to facilitate ADCP by primary $CD14^+$ monocytes was measured in
152 vitro by exposing freshly isolated human PBMCs to CHO-CoV-2-Spike cells that were pre-incubated
153 with antibody (**Figure 2g**). VIR-7831, VIR-7832 and S309-LS induced similar levels of ADCP by $CD14^+$
154 monocytes. These results indicate that VIR-7831 and VIR-7832 have the potential to trigger ADCC and
155 ADCP of cells displaying SARS CoV-2 S protein.

156 **Subneutralizing levels of VIR-7831 and VIR-7832 do not enhance virus uptake, replication or**
157 **cytokine production in vitro.** One potential concern with any antibody therapeutic targeting a viral agent
158 is the possibility of antibody-dependent enhancement (ADE). ADE is an in vivo phenomenon in which
159 the presence of an antibody worsens disease. There are several in vitro assays that may provide plausible
160 correlates for ADE in vivo, though none of these have been proven relevant to COVID-19 as to date ADE
161 has not been observed in trials of monoclonal antibodies or plasma[13,15,38,39]. ADE can occur by several
162 potential mechanisms[40]. Poorly neutralizing antibodies or subneutralizing levels of antibody could
163 theoretically facilitate enhanced virus entry and infection through Fc receptor interactions. A second
164 theoretical mechanism involves antibody-antigen complex formation leading to enhanced cytokine
165 production. A third mechanism of ADE has been observed in a porcine model of influenza where the
166 kinetics of viral fusion to the target cell was enhanced in a Fab-dependent manner by fusion-enhancing
167 non-neutralizing antibodies[41,42].

168 To explore whether VIR-7831 and VIR-7832 exhibit in vitro activities that might be related to ADE in
169 vivo, we evaluated SARS-CoV-2 replication in human cells that express FcγRs: monocyte-derived
170 dendritic cells (moDCs), peripheral blood mononuclear cells (PBMCs) and the human U937 macrophage

171 cell line (**Supplemental Figure 2a-b**). Subneutralizing concentrations of VIR-7831 and VIR-7832 were
172 precomplexed with SARS-CoV-2 (MOI =0.01) and added to target cells. Using immunostaining methods,
173 at 24 hours post-infection no productive entry of SARS-CoV-2 into moDCs, PBMCs, or U937 cells was
174 observed in the presence or absence of either mAb, while VeroE6 control cells demonstrated
175 internalization in all conditions evaluated. Reduced internalization of SARS-CoV-2 in VeroE6 cells was
176 observed at the highest concentration of VIR-7831 and VIR-7832 (p-value <0.05), indicating effective
177 virus neutralization prevented virus entry. Using a focus forming assay, virus replication and secretion of
178 infectious virus were detectable by 48 hours post-infection in VeroE6 cells, with comparable levels of
179 replication in the presence or absence of VIR-7831 or VIR-7832. However, no replication of SARS-CoV-
180 2 was detected in moDCs, PBMCs or U937 cells regardless of antibody treatment, indicating lack of
181 productive SARS-CoV-2 infection of these cells, consistent with previously published data[43].

182 To evaluate the potential for VIR-7831 and VIR-7832 to enhance cytokine release upon SARS-CoV-2
183 infection in FcγR-expressing cells, cytokines and chemokines were measured in the supernatants from
184 cells infected with SARS-CoV-2-in the presence of VIR-7831 or VIR-7832 (**Supplemental figure 2c**).
185 Levels of IFN-γ, IL-10, IL-6, IL 8, IP-10, MCP-1, and TNF-α in the supernatant were quantified by MSD
186 at 24- and 48-hours post-infection. For all cell types evaluated, cytokine/chemokine production was
187 similar between all antibody concentrations tested and the no antibody control at both 24- and 48-hours
188 post-infection. Taken together, these in vitro data indicate that neither VIR-7831 nor VIR-7832 exhibit in
189 vitro activities that have been proposed to possibly correlate with ADE in vivo.

190 **VIR-7831 and VIR-7832 have a high barrier to resistance in vitro and do not display cross-**
191 **resistance with other SARS-CoV-2 mAbs.** We next determined whether resistant variants could be
192 elicited by serial passage of SARS-CoV-2 in the presence of VIR-7832. As VIR-7831 and VIR-7832
193 differ only in the Fc region of the antibody, resistance selection experiments were conducted with VIR-
194 7832 as a proxy for both antibodies. SARS-CoV-2 was subjected to 10 passages in the presence of VIR-
195 7832 at fixed concentrations of ~10x, 20x, 50x or 100x IC_{50} (1, 2, 5, or 10 μg/mL) in VeroE6 cells. No

196 CPE was detected in wells passaged with antibody through 10 passages, while CPE was observed in the
197 no antibody control in all passages. Similarly, no virus was detected by focus forming assay at any
198 concentration of VIR-7832 through all 10 passages even at the lowest concentration tested.

199 As no viral breakthrough was observed in the fixed concentration resistance selection, a second method
200 was employed wherein SARS-CoV-2 virus was passaged in sub-IC_{50} concentrations of antibody followed
201 by subsequent passaging in the presence of increasing concentrations of mAb in an attempt to force
202 resistance emergence (**Supplemental Figure 3**). Passaging was performed in duplicate wells to account
203 for founder effects, and concentration increases for each well were based on CPE observations. Five
204 sequential passages were conducted using increasing concentrations of VIR-7832 at 0.5, 1, 2, 5 and ~10x
205 IC_{50} (0.05, 0.1, 0.2, 0.5, 1 μg/mL; **Supplemental Figure 3a**), though no CPE was observed by passages 4
206 and 5 (0.5 and 1 μg/mL, respectively) indicating that variants originally selected at the lower
207 concentrations were either unfit or susceptible to the higher concentrations of antibody. To further assess
208 whether resistance mutations could be generated, selection was restarted using passage 3 virus generated
209 with ~2x IC_{50} (0.2 μg/mL) of VIR-7832 in duplicate wells at ~2x and ~5x IC_{50} (0.2, 0.5 μg/mL),
210 generating two passage lineages (**Supplemental Figure 3b-c**).

211 Supernatants were evaluated for detectable virus at each passage by focus forming assay and cell
212 supernatants from viral passages containing detectable virus were tested in SARS-CoV-2 neutralization
213 assays to evaluate IC_{50} shifts as a marker of reduced susceptibility (**Supplemental Table 1**). With the
214 exception of passage 8, modest fold changes were observed, with shifts in IC_{50} values ranging from 5.4-
215 to 6.5-fold compared to the wild-type SARS-CoV-2 stock virus. In lineage 1, the passage 8 virus
216 displayed a >10-fold shift in IC_{50} (greater than highest concentration tested). Sequence analysis detected
217 an identical 4 amino acid insertion in the N-terminal domain (215-216insKLRS) and 5 amino acid
218 deletion in correspondence of the furin cleavage site (675-679del) in both lineages at all passages
219 sequenced, as well as the amino acid substitution E340A in lineage 1, and R682W, and V1128F in
220 lineage 2. The deletion at amino acids 675-679 has been previously described during passaging of SARS-

221 CoV-2 in tissue culture suggesting enrichment to be a result of cell culture adaptation[44] while the 215-
222 216insKLRS was detected in the input virus. Neither 215-216insKLRS nor R682W variants were highly
223 enriched with passaging (**Supplemental Table 1**) and enrichment of 675-679del and V1128F did not
224 profoundly alter the VIR-7832 IC_{50}. However, appearance of the E340A variant at 98.7% did correlate
225 with a >10-fold shift in IC_{50} suggesting this variant may confer resistance.

226 To evaluate whether amino acid variants identified in the resistance selection conferred reduced
227 susceptibility to VIR-7831 and VIR-7832, neutralization of pseudotyped viruses encoding the S variants
228 was assessed (**Supplemental Table 2**). VIR-7831 and VIR-7832 neutralized R682W and V1128F SARS-
229 CoV-2 pseudotyped virus spike variants with IC_{50} values similar to wild type (< 2-fold change in IC_{50})
230 indicating that these variants do not alter susceptibility. In contrast, E340A conferred reduced
231 susceptibility to VIR-7831 and VIR-7832 (> 100-fold change in IC_{50}) indicating that E340A is a VIR-
232 7831/VIR-7832 monoclonal antibody resistance mutation (MARM).

233 As VIR-7831/VIR-7832 demonstrated a unique in vitro resistance profile, we investigated the potential
234 for cross-resistance to MARMs that confer reduced susceptibility to the authorized monoclonal antibodies
235 bamlanivimab, imdevimab and casirivimab [10,11,45–47] using pseudotyped virus. Notably, some of these
236 mutations are found in highly prevalent variants of concern[17,30,48]. VIR-7831 effectively neutralized
237 pseudotyped viruses expressing spike MARMs that alter bamlanivimab, casirivimab and/or imdevimab
238 activity (**Table 3**). Fold changes in IC_{50} values compared to wild-type were <3-fold for 18/19 variants
239 tested. A modest 3.4-fold shift in the VIR-7831 IC_{50} was observed for the V445A variant that confers
240 reduced susceptibility to imdevimab. These data indicate that VIR-7831/VIR-7832 does not display cross-
241 resistance with currently authorized mAbs and supports the potential combination use of VIR-7831/VIR-
242 7832 with other mAb therapeutics.

243 **The VIR-7831/VIR-7832 epitope is highly conserved among SARS-CoV-2 sequences.** The parental
244 antibody of VIR-7831 and VIR-7832 (S309) binds to a highly conserved sarbecovirus epitope that is
245 potentially intolerant of variation. To investigate the current state of epitope conservation, >1,700,000

246 spike sequences from SARS-CoV-2 deposited in the GISAID database as of June 4, 2021 were examined
247 for epitope variation. More than 99.8% conservation is seen for those amino acids comprising the epitope
248 among currently available sequences for all positions including 16/23 amino acid positions that were
249 ≥99.99 conserved (**Table 4**).

250 VIR-7831 activity against viral mutants carrying single substitutions in the epitope was assessed in
251 pseudotyped virus assays. VIR-7831 effectively neutralized epitope variants at most amino acid positions
252 tested (**Table 5**). A moderate shift in activity was observed for the K356T variant (5.9-fold shift in IC_{50}).
253 Variants at two positions, E340 and P337, resulted in significant IC_{50} shifts indicating reduced
254 susceptibility to VIR-7831. Moderate shifts in potency were observed for P337H and P337T variants
255 (7.50- and 5.38-fold, respective) while more significant shifts in potency were observed for P337L/R and
256 E340A/K/G (27-fold to >276-fold). Notably, these variants are detected in a low number of sequences
257 and do not have a pattern that suggest emergence in the GISAID database (93 and 95 variant counts out of
258 >1,700,000 sequences for P337 and E340, respectively). This observation is consistent with the
259 possibility that variations at these positions come with a fitness cost to the virus.

260 **VIR-7831 reduces weight loss, total viral load and infectious virus levels in a hamster model of**
261 **SARS-CoV-2 infection.** To evaluate the efficacy of VIR-7831 in vivo, the hamster model was utilized.
262 As it was unknown what effect the LS mutation would have in the hamster, a non-LS version of VIR-
263 7831 (SGHmAb-no-LS) was used for these experiments. Hamsters were administered SGHmAb-no-LS
264 intraperitoneally at Day -1 (30, 5, 0.5 or 0.05 mg/kg) or Day -2 (15, 5, 0.5 or 0.05 mg/kg) prior to
265 intranasal SARS-CoV-2 inoculation (**Figure 3a**). Using body weight as a marker of degree of clinical
266 disease, doses of ≥5mg/kg resulted in significantly reduced weight loss at Day 4 compared to controls.
267 (**Figure 3b-e**). Significant decreases in lung viral load were also observed at ≥5mg/kg as measured by
268 RT-qPCR (**Figures f-g**). Day 4 $TCID_{50}$ measurements indicated that antibody administered at ≥0.5 mg/kg
269 resulted in significantly lower levels of infectious virus in lung tissue compared to controls (**Figure 3h-i**).
270 Notably, across these experiments, no enhancement of disease was observed in animals receiving

271 SGHmAb-no-LS based on changes in weight, viral RNA in the lungs, or $TCID_{50}$ infectious virus levels.
272 Collectively, these data indicate that VIR-7831 prevented in a dose-dependent fashion virus replication
273 and morbidity in SARS-CoV-2 challenged hamsters without signs of ADE at any dose tested.

274 **DISCUSSION**

275 Here we show the in vitro and in vivo preclinical characterization of VIR-7831 and VIR-7832, two
276 monoclonal antibodies being advanced into clinical studies[49–51]. Both antibodies demonstrate high-affinity
277 binding to S in vitro, including on the surface of cells, and effectively neutralize wildtype SARS-CoV-2
278 in a live virus assay. VIR-7831 and VIR-7832 retain activity against the Alpha (B.1.1.7), Beta (B.1.351),
279 Gamma (P.1), Delta (B.1.617.2) and Kappa (B.1.617.1) variants in an authentic virus system, consistent
280 with data using pseudotyped viruses. VIR-7831 bind C1q, activate FcγRs and demonstrate ADCC and
281 ADCP in vitro. Experiments in the hamster model of SARS-CoV-2 infection show proof-of-concept
282 efficacy in vivo. Notably, in vitro and in vivo data did not provide any supporting evidence that these
283 antibodies would demonstrate ADE in a clinical setting.

284 That VIR-7831 and VIR-7832 retain activity against spike variants in authentic virus and pseudotyped
285 virus assays is a key finding at this stage of the pandemic. With the increased transmissibility and
286 potential for more severe disease observed with these viruses, the availability of therapeutic or
287 prophylactic mAbs that remains active against variants is essential. In addition to retaining activity
288 against all current WHO VOCs and VOIs, in pseudotyped virus experiments VIR-7831 showed no
289 significant cross-resistance with variants that reduce the activity of authorized mAbs. These data
290 additionally demonstrate the uniqueness of VIR-7831 and VIR-7832 and further highlight the utility VIR-
291 7831 and VIR-7832 could have, alone or in combination, as clinical agents.

292 Notably, even at this stage of the pandemic, the VIR-7831/VIR-7832 epitope remains highly conserved
293 among available sequences of circulating virus with ≥99.8% conservation of epitope amino acids. This is
294 consistent with the value of the strategy used for isolation of monoclonal antibodies that neutralize both

295 SARS-CoV and SARS-CoV-2 based on the idea that these two virulent human viruses are
296 phylogenetically divergent within the sarbecovirus subgenus. Furthermore, MARMs identified at
297 positions P337 and E340 are present at very low levels among current sequences. That amino acids P337
298 and E340 remain ≥99.99% conserved at this stage of the pandemic indicates that variants at these
299 positions may confer disadvantageous effects on the virus, consistent with the conservation of this epitope
300 across the sarbecovirus family[21].

301 Viral variants of concern for RBM-targeting mAbs are quickly spreading[53]. The vaccines presently being
302 deployed around the world generate high-titer neutralizing antibodies that target the S protein RBM.
303 Importantly, the RBM is highly immunodominant for responses to natural infection[54]. Vaccine-induced
304 and convalescent immunity may therefore potentially put further mutational pressure on the RBM
305 sequence to evade such antibody responses. In contrast, antibody responses overlapping with the VIR-
306 7831/VIR-7832 epitope are limited after infection [54], possibly because of the shielding effect of the highly
307 conserved N343 glycan. In this regard the epitope may face less vaccine- or infection-generated immune
308 pressure, potentially preserving this conserved epitope long-term.

309 Recent data have indicated that the cells used to generate live virus stocks and overexpression of
310 ACE2/TMPRSS2 in target cells used for assays can affect mAb activity in vitro[29,55]. The VIR-7831/VIR-
311 7832 parental antibody S309 seems particularly sensitive to in vitro methods using ACE2 overexpressing
312 cells[55]. It is therefore notable that VIR-7831 displays significant efficacy in an in vivo proof-of-concept
313 SARS-CoV-2 infection experiment using hamsters despite the fact that patterns of engagement of hamster
314 FcRs by human IgG1 antibodies may not reflect patterns of human IgG1 antibodies with their cognate
315 human FcRs. These findings argue that in vitro data derived from such ACE2 and/or TMPRSS2
316 overexpression cell lines do not accurately reflect the in vivo antiviral capacity of tested mAbs.
317 Furthermore, that the significant in vivo effects of VIR-7831 in the hamster model likely occurred in the
318 absence of full effector functions due to species-specific interactions between antibodies and FcRs, argues

319 that effects in COVID-19 patients incorporating both the neutralization capacity of the antibody plus the
320 ability to harness the strength of the immune system could lead to positive clinical outcomes.

321 The clinical potential of VIR-7832, with the inclusion of the GAALIE Fc mutation, is of special interest
322 in the context of SARS-CoV-2 infection. Previously published data by the Ravetch laboratory comparing
323 the in vivo efficacy of a hemagglutinin-targeting mAb with and without inclusion of the GAALIE
324 mutation in a transgenic humanized FcγR mouse model of influenza infection demonstrated superior
325 efficacy of the GAALIE-containing antibody in both therapeutic and prophylactic experiments[26]. These
326 effects were mediated by protective $CD8^+$ T cell responses elicited by the GAALIE antibody. Clinical
327 data examining the contribution of the adaptive immune response in SARS-CoV-2 infection indicate that
328 poor T cell induction correlates with severe disease (reviewed in [56]). Thus, the potential for VIR-7832 to
329 augment the T cell response to SARS-CoV-2 infection could conceivably play a crucial role in limiting
330 progression to severe COVID-19 disease or in treatment of severe established disease. This latter
331 possibility is supported by recent publications showing that monoclonal antibodies with effector functions
332 are especially effective in the therapeutic setting via recruitment of tissue-protective monocyte functions
333 [19], and that potency of antibodies in the pre-clinical mouse model does not correlate with in vitro
334 neutralizing activity of antibodies[18].

335 Taken together, these data indicate that VIR-7831 and VIR-7832 could play a powerful role in the fight
336 against COVID-19 through the dual action of broadly neutralizing activity paired with engagement of the
337 immune system through effector function capabilities.

338

339 **METHODS**

340 **Cells.** Vero E6 cells (ATCC) and Lenti-X 293T cells (Takara) were cultured in Dulbecco's Modified
341 Eagle's medium (DMEM), 10% FBS, 1x Penicillin-Streptomycin at 37°C, 5% CO_2.

342 **Monoclonal Antibodies.** VIR-7831 and VIR-7832 were produced at WuXi Biologics (China). SGHmAb-
343 no-LS, S309-LS, and S309-GRLR were produced at Humabs Biomed SA, a subsidiary of Vir
344 Biotechnology (Bellinzona, Switzerland) in expiCHO cells transiently co-transfected with plasmids
345 expressing the heavy and light chain, as previously described [57].

346 **Virus. S**ARS-CoV-2 isolates USA-WA1/2020, UK/VUI/3/2020, hCoV-19/South Africa/KRISP-
347 K005325/2020, hCoV-19/Japan/TY7-503/2021, hCoV-19/USA/CA-SU-15-S02/2021 and hCoV-
348 19/USA/PHC658/2021 were obtained from BEI Resources. To propagate SARS-CoV-2, VeroE6 or
349 VeroE6-TMPRSS2 cells were seeded at $10X10^6$ cells in T175 flasks in growth media and infected the
350 next day at a MOI of 0.001 in virus propagation media. Virus was adsorbed for 1 hour at 37°C. Virus
351 inoculum was removed, flasks were washed once with PBS, 25 mL of infection media was added to the
352 cells and flasks were incubated at 37°C. Supernatants were collected at 48 hours post-infection once
353 cytopathic effect was visible, centrifuged at 500 x g for 5 minutes, followed by a second centrifugation at
354 1000 x g for 5 minutes. Clarified supernatants were then aliquoted and stored at -80°C. Virus titers were
355 determined using a plaque assay on VeroE6 cells, using standard methods. Briefly, 10-fold dilutions of
356 virus stock were incubated in 6 well plates with 2.4% colloidal cellulose overlay for 24 hours. Cells were
357 fixed with 4% PFA for 30 minutes at room temperature (RT), permeabilized with 0.125% Triton X-100,
358 stained with anti-SARS-CoV-2 nucleocapsid antibody at 1:5000 and goat anti-rabbit IgG HRP at 1:5000.
359 Plaque forming units (PFU) were visualized with TrueBlue reagent.

360 **In vitro binding ELISA.** For the ELISA assay, 96-well plates were coated with 100 µl/well recombinant
361 SARS-CoV2 RBD diluted in assay diluent (1% BSA/PBS) at a final concentration of 2 µg/mL and
362 incubated overnight at 4°C. Plates were washed three times with 300 µl/well wash buffer using an
363 automated washer. Assay diluent (100 µl/well) was added to block the plates and incubated for 1 hour at
364 room temperature (RT) with shaking. Assay diluent was removed, and plates washed three times with
365 wash buffer. Serial 1:3 dilutions of mAb (concentration range from 6 µg/mL to 0.33 ng/mL) in assay
366 diluent were dispensed at 100 µl/well and incubated 1 hour at RT with shaking, then washed three times

367 with wash buffer. The HRP-conjugated secondary antibody reagent (1:5,000 dilution in assay diluent)
368 was added to each well (100 µl/well) and incubated for 1 hour at RT with shaking. After three washes
369 with wash buffer, 100 µl/well of 2-component TMB peroxidase substrate solution was dispensed in each
370 well and developed for 5 minutes at RT. The reaction was stopped with 100 µL/well 1M H_2SO_4 and the
371 OD was read immediately at 450 nm on a SpectraMax M5 Microplate reader. EC_{50} values were calculated
372 using non-linear regression of log (agonist) versus response in Graph Pad Prism.

373 **Spike binding affinity quantification by SPR.** Antibody was diluted to 2 µg/mL (1 mL) in HBS-EP+
374 buffer and injected at 10 µL/min for 30 seconds across one flow cell of a CM5 sensor chip immobilized
375 with anti-human Fc antibody docked in a Biacore T200. SARS-CoV2-RBD diluted in HBS-EP+ buffer
376 was then injected at a single concentration, 1:3 dilutions from 100 nM to 3.7 nM, across both the flow cell
377 containing captured the antibody as well as a reference flow cell containing only anti-human Fc antibody.
378 Binding was measured with a flow rate of 30 µL/min and an injection time of 600 seconds; dissociation
379 was monitored for 1800 seconds after injection. Data were collected at 10 Hz. After each binding
380 measurement, regeneration reagent was injected to prepare the surface for a new cycle. Experiments were
381 performed at 25°C, with the samples held at 15 °C in the instrument prior to injection.

382 **Measurement of Binding to Human Fcγ Receptors by SPR.** Binding of VIR-7831 and VIR-7832 to
383 human recombinant FcγRs was measured by surface plasmon resonance (SPR) on a Biacore T200.
384 Briefly, Biotin CAPture Reagent (modified streptavidin) was injected across all flow cells of a CAP
385 sensor chip docked in a Biacore T200. Biotinylated Fc receptors at 1 µg/mL were injected across a single
386 flow cell at 10 µL/min for 60 seconds (one receptor per flow cell), with one flow cell reserved as a
387 reference surface. VIR 7831 or VIR-7832 at 100 µg/mL (diluted in HBS-EP+) were injected across all
388 flow cells for 200 seconds using a flow rate of 30 µL/min and association was monitored. Dissociation
389 was monitored for another 200 seconds after injection. Data was collected at 10 Hz. After each binding
390 measurement, CAP Regeneration reagent was injected to prepare the surface for a new cycle.
391 Experiments were performed at 25°C, with the samples held at 15°C in the instrument prior to injection.

392 **Measurement of Binding to Human Complement Protein C1q.** Binding of VIR-7831 and VIR-7832 to
393 human complement was measured by biolayer interferometry (BLI) using an Octet Red96 instrument
394 (FortéBio). Briefly, anti-human Fab (CH1-specific) sensors were used to capture VIR-7831 and VIR-
395 7832 at 10 µg/ml for 10 minutes. The IgG-loaded sensors were then exposed to kinetics buffer containing
396 3 µg/ml of purified human C1q for 4 minutes, followed by a dissociation step in the same buffer for
397 additional 4 minutes. Association and dissociation profiles were measured in real time as changes in the
398 interference pattern.

399 **Binding to Cell Surface Expressed SARS-CoV-2 Spike Protein.** The SARS-CoV-2 spike protein
400 coding sequence (YP_009724390.1, Wuhan-Hu-1 strain) was cloned into a cell expression plasmid under
401 the control of the human CMV promoter (phCMV1) to generate phCMV1 WT spike. ExpiCHO-S cells
402 were seeded the day before transfection at 3 x 10^6 cells/mL in ExpiCHO Expression Medium.
403 Immediately before transfection, the cells were seeded at 6 x 10^6 cells cells/mL in a volume of 15 mL in
404 125 mL shake flasks. Six µg of phCMV1 WT spike plasmid or vector control were diluted in 1.2 mL of
405 iced OptiPRO SFM., followed by addition of 48 µL of ExpiFectamine CHO Reagent and complexing for
406 1 minute at RT. The transfection mixture was added dropwise to cells with gentle swirling. Cells were
407 then incubated at 37°C, 8% CO2 with shaking for 42 hours. At 42 hours post-transfection, ExpiCHO-S
408 cells were harvested, washed twice with FACS buffer and resuspended at a concentration of 1.0 x 10^6
409 cell/mL in PBS. Cells (5 x 10^4 cells in 50 µl/wells) were dispensed into a 96-well V-bottom plate.
410 Antibody was serially diluted (1:4, 10 points) starting at a concentration of 10 µg/mL. Cells were pelleted
411 at 300 x g for 5 minutes and resuspended in 50 µL/well of antibody serial dilutions and plates were
412 incubated for 45 mins on ice. Cells were washed twice in FACS buffer. Alexa Fluor 647-labelled Goat
413 Anti-Human IgG secondary Ab was diluted 1:750 in FACS buffer and 50 µL was added to the cell pellet
414 for 15 min on ice. Cells were washed twice with FACS buffer, resuspended in 1% PFA. Data was
415 acquired by flow cytometry (CytoFlex LX).

416 **Pseudotyped virus production.** Lenti-X™ 293T cells were seeded in 10-cm dishes for 80% next day
417 confluency. The next day, cells were transfected with the plasmid pcDNA3.1(+)-spike-D19 (encoding the
418 SARS-CoV-2 spike protein) or pcDNA3.1(+)-spike-D19 variants using the transfection reagent TransIT-
419 Lenti according to the manufacturer's instructions. One day post-transfection, cells were infected with
420 VSV-luc (rVSVΔG; Kerafast) at an MOI of 3. The cell supernatant containing SARS-CoV-2 pseudotyped
421 virus was collected at day 2 post-transfection, centrifuged at 1000 x g for 5 minutes to remove cellular
422 debris, aliquoted and frozen at -80°C.

423 **In Vitro Neutralization of SARS-CoV-2 Pseudotyped Virus.** VeroE6 cells were seeded into flat
424 bottom tissue culture 96-well plates at 20,000 cells/well and cultured overnight at 37°C. Twenty-four
425 hours later, 9-point 1:4 serial dilutions of VIR-7831 were prepared in infection medium and each dilution
426 was tested in triplicate per plate (range: 20,000 to 0.3 ng/mL final concentration). SARS-CoV-2 virus
427 stock was diluted in infection media for a final concentration of 2000 plaque forming units per well (MOI
428 0.1). Antibody dilutions were added to virus and incubated for 30 minutes at 37°C. Media was removed
429 from the VeroE6 cells, mAb-virus complexes were added, and cells were incubated at 37°C. At 6 hours
430 post-infection, cells were fixed with 250 µL 4% PFA, incubated for 30 minutes at RT, then washed 3
431 times with PBS to remove residual PFA. The cells were permeabilized with 50 µL of 0.125% Triton X-
432 100 in PBS for 30 minutes at RT. The blocking buffer was removed, 50 µL of SARS-CoV-2 nucleocapsid
433 antibody at 1:2,000 in blocking buffer was added, and plate was incubated for 1 hour at RT. Plates were
434 washed three times with PBS and then incubated for 1 hour at RT with 50 µL/well of goat anti-rabbit-
435 Alexa647 secondary antibody at a final dilution of 1:1,000 mixed with 2 ug/mL Hoechst dye in blocking
436 buffer. After washing 5 times with PBS, 100 µL of fresh PBS was added for imaging. Plates were imaged
437 on a Cytation5 plate reader. Whole well images were acquired (12 images at 4X magnification per well)
438 and nucleocapsid-positive cells were counted using the manufacturer's software.

439 **Live virus neutralization.** VeroE6 cells were seeded into flat bottom tissue culture 96-well plates at
440 20,000 cells/well and cultured overnight at 37°C. Twenty-four hours later, 9-point 1:4 serial dilutions of

441 VIR-7831 were prepared in infection medium and each dilution was tested in triplicate per plate (range:
442 20,000 to 0.3 ng/mL final concentration). SARS-CoV-2 virus stock was diluted in infection media for a
443 final concentration of 2000 plaque forming units per well (MOI 0.1). Antibody dilutions were added to
444 virus and incubated for 30 minutes at 37°C. Media was removed from the VeroE6 cells, mAb-virus
445 complexes were added, and cells were incubated at 37°C. At 6 hours post-infection, cells were fixed with
446 250 µL 4% PFA, incubated for 30 minutes at RT, then washed 3 times with PBS to remove residual PFA.
447 The cells were permeabilized with 50 µL of 0.125% Triton X-100 in PBS for 30 minutes at RT. The
448 blocking buffer was removed, 50 µL of SARS-CoV-2 nucleocapsid antibody at 1:2,000 in blocking buffer
449 was added, and plate was incubated for 1 hour at RT. Plates were washed three times with PBS and then
450 incubated for 1 hour at RT with 50 µL/well of goat anti-rabbit-Alexa647 secondary antibody at a final
451 dilution of 1:1,000 mixed with 2 ug/mL Hoechst dye in blocking buffer. After washing 5 times with PBS,
452 100 µL of fresh PBS was added for imaging. Plates were imaged on a Cytation5 plate reader. Whole well
453 images were acquired (12 images at 4X magnification per well) and nucleocapsid-positive cells were
454 counted using the manufacturer's software..

455 **Determination of Viral Titer by Focus-Forming Assay.** One day prior to infection, $1.2X10^4$ VeroE6
456 cells were plated in black-walled, clear bottomed 96-well plates. Virus samples were diluted 1:5 in
457 infection media and adsorbed onto VeroE6 cells for one hour at 37°C. The cells were washed once and
458 overlaid with 1% methylcellulose/serum-containing media. At 24 hours post-infection, the
459 methylcellulose overlay was removed, and cells were washed with PBS. Cells were fixed with 4% PFA,
460 incubated for 30 minutes at RT, then washed with PBS to remove residual PFA. The cells were
461 permeabilized with 50 µL of 0.25% Triton X-100 in PBS for 30 minutes at RT. The Triton X-100 was
462 removed, cells were washed twice with PBS, and incubated with 50 µL of SARS-CoV-2 nucleocapsid
463 antibody at 1:2,000 in blocking buffer for one hour at RT. Plates were washed three times with PBS and
464 then incubated for one hour at RT with 50 µL/well of goat anti-rabbit-Alexa647 secondary antibody at
465 1:1,000 in blocking buffer. After washing three times with PBS, 50 µL of Hoechst dye at 1:1,000 in PBS

466 was added for imaging. Plates were imaged on a Cytation5 plate reader. Whole well images were
467 acquired (12 images at 4X magnification per well) and nucleocapsid-positive foci were counted using the
468 manufacturer's software and used to determine focus-forming units/mL supernatant (FFU/mL).

469 **Determination of mAb-Dependent Activation of Human FcγRIIa, FcγRIIIa or FcγRIIb.** VIR-7831,
470 VIR-7832, S309-LS, and a control mAb with abrogated FcγR binding, S309-GRLR, were serially diluted
471 6-fold in assay buffer from 10,000 ng/ml to 0.006 ng/ml. Nine-point serial dilutions of mAbs were
472 incubated with 12,500 (for FcγRIIIa and FcγRIIb) or 10,000 (for FcγRIIa) CHO-CoV-2-Spike cells per
473 96-plate well in a white, flat-bottom plate for 15 minutes at room temperature. Jurkat effector cells
474 expressing indicated FcγRs and stably transfected with an NFAT-driven luciferase gene were thawed,
475 diluted in assay buffer, and added to the plate at an effector to target cell ratio of 6:1 for FcRγIIIa and
476 FcγRIIb or 5:1 for FcγIIa. Control wells were also included that were used to measure antibody-
477 independent activation (containing target cells and effector cells but no antibody) and background
478 luminescence of the plate (wells containing assay buffer only). Plates were incubated for 18 hours at 37°C
479 with 5% CO2. Activation of human FcγRs in this bioassay results in the NFAT-mediated expression of
480 the luciferase reporter gene. Luminescence was measured with a luminometer after adding the Bio
481 GloTM Luciferase Assay Reagent according to the manufacturer's instructions. To control for
482 background, the mean of the relative luminescence units (RLU) values in wells containing only Assay
483 Buffer was calculated and subtracted from all data points. Data were expressed as the average of RLUs
484 over the background

485 **Determination of NK-Cell Mediated Antibody-Dependent Cellular Cytotoxicity.** Primary NK cell
486 activation was tested using freshly isolated cells from two previously genotyped donors expressing
487 homozygous low affinity (F158) or high affinity (V158) FcγRIIIa. Serial dilutions of mAbs (serially
488 diluted 10-fold in AIM-V Medium from 40,000 ng/ml to 0.075 ng/ml) were incubated with 7,500 CHO-
489 CoV-2 Spike cells per well of a 96 well round-bottom plate for 10 minutes. Target cell and antibody
490 mixtures were then incubated with primary human NK cells as effectors at an effector-to-target ratio of

491 10:1. ADCC was measured using lactate dehydrogenase (LDH) release as a readout according to the
492 manufacturer's instructions (Cytotoxicity Detection Kit (LDH), Roche) after 4 hours of incubation at
493 37°C. In brief, plates were centrifuged for 4 minutes at 400 x g, and 35 µl of supernatant was transferred
494 to a flat 384 well plate. LDH reagent was prepared and 35 µl were added to each well. Using a kinetic
495 protocol, the absorbance at 490 nm and 650 nm was measured once every 2 minutes for 8 minutes, and
496 the slope of the kinetics curve was used as result. The percent specific lysis was determined by applying
497 the following formula: (specific release – spontaneous release) / (maximum release - spontaneous release)
498 x 100.

499 **Determination of Monocyte-Mediated Antibody-Dependent Cellular Phagocytosis.** ADCP assays
500 were performed using human PBMCs freshly isolated from whole blood. CHO CoV-2-Spike cells were
501 used as target cells and were fluorescently labeled with PKH67 Fluorescent Cell Linker Kit (Sigma
502 Aldrich) prior to incubation with mAbs, according to manufacturer's instructions. Serial dilutions of
503 mAbs (serially diluted 5-fold from 5,000 ng/ml to 0.32 ng/ml in RPMI-1640 + L-glutamine supplemented
504 with 10% Hyclone FBS + 2x anti-anti (antibiotic-antimycotic)) were incubated with 10,000 CHO-CoV-2-
505 Spike cells per well of a 96 well polypropylene plate for 10 minutes. Primary PBMCs were fluorescently
506 labeled with Cell Trace Violet according to the manufacturer's instructions. Target cell and antibody
507 mixtures were then incubated with labeled PBMCs at an effector-to-target ratio of 16:1. After an
508 overnight incubation at 37°C, monocytes were stained with anti-human CD14-APC antibody (BD
509 Pharmingen). Antibody-mediated phagocytosis was determined by flow cytometry, gating on CD14+
510 cells that were double positive for cell trace violet and PKH67. Raw data were exported from the flow
511 cytometer into the flow cytometry analysis software FlowJo v10 (Becton Dickinson) for gating and
512 determination of the percentage of $CD14^+$ cells that were also double positive for cell trace violet and
513 PKH67. Cells expressing only cell trace violet or only PKH67 were used to set the positive staining gates.

514 **In vitro resistance selection.** The selection of variants in the presence of increasing concentrations of
515 VIR-7832 was conducted in VeroE6 cells. The day before infection, 6 x 10^4 VeroE6 cells were seeded in

516 24 well plates and incubated overnight at 37°C. The next day, 600 focus forming units (FFU) of SARS-
517 CoV-2 virus (MOI = 0.01) was incubated with 0.5X IC_{50} of VIR-7832 (0.05 µg/mL) at 37°C for one hour
518 in infection media. The mAb-virus complexes were adsorbed on VeroE6 cells for one hour at 37°C in
519 duplicate wells. After adsorption, cells were washed with DMEM and overlaid with infection media
520 containing 0.05 µg/mL VIR-7832. Control wells infected without antibody were included with each
521 passage. Infected cells were monitored visually for CPE daily. In general, when infected cells exhibited ≥
522 50% CPE, the culture supernatants were harvested, diluted 1:200, and added to fresh VeroE6 cells in 24-
523 well plates with equivalent or increasing concentrations of VIR-7832. At each passage, supernatant was
524 aliquoted and frozen at -80°C for titer and neutralization analyses.

525 **In vitro assessment of potential for ADE.** VeroE6 cells were plated at $1.25X10^4$ cells/well one day prior
526 to infection. For each independent experiment, moDCs and PBMCs from five unique moDC donors and
527 six unique PBMC donors were used, with three unique donors used for each independent experiment.
528 Cryopreserved monocytes from unique donors were differentiated into moDCs for six days using human
529 moDC differentiation media according to the manufacturer's protocol. Cryopreserved PBMCs from
530 unique donors are thawed in the presence 0.3 mg/mL DNase and cultured in media for one day prior to
531 infection. On the day of infection, moDCs, PBMCs, and U937 cells were counted and plated at $7.5X10^4$
532 cells/well.

533 To examine viral entry, 24 hours post-infection, cells were fixed with 4% PFA, incubated for 30 minutes
534 at RT, then washed with PBS to remove residual PFA. The cells were permeabilized with 50 µL of 0.25%
535 Triton X-100 in PBS for 30 minutes at RT. The Triton X-100 was removed, cells were washed twice with
536 PBS, and incubated with 50 µL of SARS-CoV-2 nucleocapsid antibody at 1:2,000 in blocking buffer for
537 one hour at RT. Plates were washed three times with PBS and then incubated for one hour at RT with 50
538 µL/well of goat anti-rabbit-Alexa647 secondary antibody at 1:1,000 in blocking buffer. After washing
539 three times with PBS, 50 µL of Hoechst dye at 1:1,000 in PBS was added for imaging. Plates were
540 imaged on a Cytation5 plate reader. Whole well images were acquired (12 images at 4X magnification

541 per well) and nucleocapsid-positive cells were counted using the manufacturer's software. The percent of
542 nucleocapsid+ cells was quantified using the Gen5 Imager software (Biotek, Vermont) as number of
543 Cy5+ cells, [(nucleocapsid+ cells)/number of Hoechst+ cells (total cells)]x100. Data was analyzed using
544 Prism v8.00 (GraphPad Software, La Jolla California USA, www.graphpad.com).

545 In order to quantify chemokines and cytokines from supernatants in a BSL2 laboratory, supernatants were
546 inactivated by 10 minutes exposure to UVC light at 5,000 µJ/cm2. Supernatants were diluted 1:5 in
547 infection media and levels of cytokines/chemokines were quantified using the U-plex 96-well assay
548 according to the manufacturer's protocol (Meso Scale Diagnostics, Rockville, MD). Quantification of
549 cytokines and chemokines were determined based on an 8-point standard curve in duplicate, provided by
550 the manufacturer. Cytokine data was analyzed using the Discovery Workbench v4.0.13 software (Meso
551 Scale Diagnostics). Data was graphed and statistical analyses were conducted using Prism software.

552 **Sequencing of SARS-CoV-2 Spike Gene.** To isolate nucleic acid from the supernatant of viral passages,
553 120 µL of cell supernatant was added to 360 µL of Trizol and stored at -80°C for further analysis. Trizol
554 collected samples from viral passages where a shift in neutralization > 2-fold relative to wild type was
555 detected were subjected to RNA isolation using PureLink RNA Mini Kit with the incorporation of on-
556 column PureLink DNase Treatment, following manufacturer's instructions. Reverse transcription
557 reactions were performed with 6 µL of purified RNA and oligoT primers using the NEB ProtoScript II
558 First Strand cDNA Synthesis kit, according to manufacturer's instructions. The resulting cDNA was used
559 as a template for PCR amplification of the spike gene using the KapaBiosystems polymerase (KAPA HiFi
560 HotStart ReadyMix) with primers 5' aattatcttggcaaaccacg-3' and 5' tgaggcttgtatcggtatcg-3'.
561 Amplification conditions included an initial 3 minutes at 95°C, followed by 28 cycles with 20 seconds at
562 98°C, 15 seconds at 62°C and 72°C for 2 minutes, with a final 4 minutes at 72°C. PCR products were
563 purified using AMPure XP beads following manufacturer's instructions. The size of the amplicon was
564 confirmed by analyzing 2 µL of PCR products using the Agilent D5000 ScreenTape System. Products
565 were quantified by analyzing 1 µL with the Quant-iT dsDNA High-Sensitivity Assay Kit. Twenty ng of

566 purified PCR product was used as input for library construction using the NEBNext Ultra II FS DNA
567 Library Prep kit following manufacturer's instructions. DNA fragmentation was performed for 13
568 minutes. NEBNext Multiplex Oligos for Illumina Dual Index Primer Set 1 was used for library
569 construction, with a total of 6 PCR cycles. Libraries size was determined using the Agilent D1000
570 ScreenTape System and quantified with the Quant iT dsDNA High-Sensitivity Assay Kit. Equal amounts
571 of each library were pooled together for multiplexing and 'Protocol A: Standard Normalization Method'
572 of the Illumina library preparation guide was used to prepare 8 pM final multiplexed libraries with 1%
573 PhiX spike-in for sequencing. The MiSeq Reagent Kit v3 (600-cycle) was used for sequencing the
574 libraries on the Illumina MiSeq platform, with 300 cycles for Read 1, 300 cycles for Read 2, 8 cycles for
575 Index 1, and 8 cycles for Index 2.

576 **Bioinformatics Analysis of Conservation.** Available genome sequences for SARS-CoV-2 were
577 downloaded from Global Initiative on Sharing All Influenza Data (GISAID; https://www.gisaid.org/) on
578 June 4, 2021. Bat and pangolin sequences were removed to yield human-only sequences. The spike open
579 reading frame was localized by aligning the reference protein sequence (NCBI reference sequence:
580 YP_009724390.1) to the genomic sequence of isolates with Exonerate v.2.4.0. Coding nucleotide
581 sequences were translated in silico using seqkit v.0.12.0. Multiple sequence alignment was performed
582 using MAFFT v.7.455. Variants were determined by comparison of aligned sequences to the reference
583 sequence using the R v3.6.3/Bioconductor v.3.10 package Biostrings v.2.54.0.

584 **In vivo studies.** Syrian golden hamster studies were conducted at Lovelace Biomedical (Albuquerque,
585 NM). Twelve- to sixteen-week-old male hamsters were interperitoneally administered a non-LS version
586 of VIR-7831 (SGHmAb-no-LS), control antibody or diluent Day -1 or Day -2 prior to virus challenge.
587 Animals were inoculated intranasally at Day 0 with 7.4×10^4 $TCID_{50}$ with SARS-CoV-2 (isolate USA-
588 WA1/2020). Animals were also weighed once daily in the morning beginning on study Day -10 and
589 continuing until the end of the study. Following euthanasia, RT-qPCR was performed on lung

590 homogenates using quantitative real-time PCR methods targeting the SARS-CoV-2 N gene and the
591 median tissue culture infections dose ($TCID_{50}$) was determined per Lovelace internal methodology.

592 **Author Contributions**

593 Conceived studies: A.L.C, C.H-D., F.A.P, D.M., M.S., L.S., A.T., L.A.P., S.H., G.S., H.W.V., D.C., C.M.H.
594 Designed studies and experiments: A.L.C, C.H.D., F.A.P, D.M., M.S., M.L.A., E. D., B.G., J.D., L.R.,A.C., A.S.,
595 R.S., J.W., N.C., E.C., S.L., C.C., D.P., C.S., J.N., A.P., A.W., L.S., A.T., L.A.P., S.H., G.S., H.W.V., D.C., C.M.H.
596 Performed experiments: D.M., M.S., M.L.A., B.G., J.D., E.D., A.S., L.R., H.T., J.D., S.S., D.P., C.S., J.N., B.S.,
597 S.B., J.W., J.Z., H.K., A.C., M.M-R., A.P., A.W., N.C., E.C. Analyzed and interpreted data: A.L.C., C.H-D., F.A.L.,
598 D.M., M.S., M.L.A., B.G., J.D., D.P., C.S., J.N., E.L., A.S., R.S., L.R., H.T., B.S., S.B., J.W., J.Z., H.K., A.C., M. M-
599 R., N.C., E.C., S.L., A.W., C.C., L.S., A.T., S.H., G.S., H.W.G, D.C., C.M.H. Prepared the manuscript with input
600 from all authors: A.L.C., G.S., A.T., L.P., D.C., H.W.G., C.M.H.

601 **Competing interests**

602 Some authors are current or former employees of Vir Biotechnology or Humabs BioMed SA (a fully-
603 owned subsidiary of Vir Biotechnology) and may hold shares in Vir Biotechnology. H.W.V. is a founder of
604 PierianDx and Casma Therapeutics.

605

606 **REFERENCES**

607

608 1. WHO Coronavirus Disease (COVID-19) Dashboard | WHO Coronavirus Disease (COVID-19)
609 Dashboard. https://covid19.who.int/.

610 2. Levin, A. T. *et al.* Assessing the age specificity of infection fatality rates for COVID-19:
611 systematic review, meta-analysis, and public policy implications. *Eur J Epidemiol* **35**, 1123–
612 1138 (2020).

613 3. Dennis, A. *et al.* Multi-organ impairment in low-risk individuals with long COVID.
614 doi:10.1101/2020.10.14.20212555.

615 4. Murphy, J. *et al.* Psychological characteristics associated with COVID-19 vaccine hesitancy
616 and resistance in Ireland and the United Kingdom. *Nat Commun* **12**, 29 (2021).

617 5. Khubchandani, J. *et al.* COVID-19 Vaccination Hesitancy in the United States: A Rapid
618 National Assessment. *J Commun Health* 1–8 (2021) doi:10.1007/s10900-020-00958-x.

619 6. Sallam, M. *et al.* High Rates of COVID-19 Vaccine Hesitancy and Its Association with
620 Conspiracy Beliefs: A Study in Jordan and Kuwait among Other Arab Countries. *Nato Adv Sci*
621 *Inst Se* **9**, 42 (2021).

622 7. Tegally, H. *et al.* Emergence and rapid spread of a new severe acute respiratory syndrome-
623 related coronavirus 2 (SARS-CoV-2) lineage with multiple spike mutations in South Africa.
624 *medRxiv* (2020) doi:10.1101/2020.12.21.20248640.

625 8. Naveca, F. *et al.* Phylogenetic relationship of SARS-CoV-2 sequences from Amazonas with
626 emerging Brazilian variants harboring mutations E484K and N501Y in the Spike protein -
627 SARS-CoV-2 coronavirus / nCoV-2019 Genomic Epidemiology - Virological.
628 https://virological.org/t/phylogenetic-relationship-of-sars-cov-2-sequences-from-amazonas-with-
629 emerging-brazilian-variants-harboring-mutations-e484k-and-n501y-in-the-spike-protein/585
630 (2011).

631 9. Rambaut, A. *et al.* Preliminary genomic characterisation of an emergent SARS-CoV-2 lineage
632 in the UK defined by a novel set of spike mutations - SARS-CoV-2 coronavirus / nCoV-2019
633 Genomic Epidemiology - Virological. https://virological.org/t/preliminary-genomic-
634 characterisation-of-an-emergent-sars-cov-2-lineage-in-the-uk-defined-by-a-novel-set-of-spike-
635 mutations/563 (2020).

636 10. Bamlanivimab EUA Letter of Authorization Reissue 02092021.
637 https://www.fda.gov/media/143603/download.

638 11. Casirivimab and Imdevimab EUA Fact Sheet for Healthcare Providers.
639 https://www.fda.gov/media/143892/download.

640 12. Lilly's neutralizing antibody bamlanivimab (LY-CoV555) prevented COVID-19 at nursing
641 homes in the BLAZE-2 trial, reducing risk by up to 80 percent for residents.
642 https://investor.lilly.com/node/44291/pdf.

643 13. Gottlieb, R. L. *et al.* Effect of Bamlanivimab as Monotherapy or in Combination With
644 Etesevimab on Viral Load in Patients With Mild to Moderate COVID-19. *Jama* **325**, 632–644
645 (2021).

646 14. Chen, P. *et al.* SARS-CoV-2 Neutralizing Antibody LY-CoV555 in Outpatients with Covid-
647 19. *New Engl J Med* (2020) doi:10.1056/nejmoa2029849.

648 15. Weinreich, D. M. *et al.* REGN-COV2, a Neutralizing Antibody Cocktail, in Outpatients with
649 Covid-19. *New Engl J Med* **384**, 238–251 (2020).

650 16. Starr, T. N. *et al.* Prospective mapping of viral mutations that escape antibodies used to treat
651 COVID-19. *Science* **371**, 850–854 (2021).

652 17. Wang, P. *et al.* Increased Resistance of SARS-CoV-2 Variants B.1.351 and B.1.1.7 to
653 Antibody Neutralization. *Biorxiv* 2021.01.25.428137 (2021) doi:10.1101/2021.01.25.428137.

654 18. Schäfer, A. *et al.* Antibody potency, effector function, and combinations in protection and
655 therapy for SARS-CoV-2 infection in vivo. *J Exp Med* **218**, (2020).

656 19. Winkler, E. S. *et al.* Human neutralizing antibodies against SARS-CoV-2 require intact Fc
657 effector functions and monocytes for optimal therapeutic protection. *Biorxiv* 2020.12.28.424554
658 (2020) doi:10.1101/2020.12.28.424554.

659 20. Bournazos, S. & Ravetch, J. V. Fcγ Receptor Function and the Design of Vaccination
660 Strategies. *Immunity* **47**, 224–233 (2017).

661 21. Pinto, D. *et al.* Cross-neutralization of SARS-CoV-2 by a human monoclonal SARS-CoV
662 antibody. *Nature* **583**, 290–295 (2020).

663 22. Pinto, D. *et al.* Cross-neutralization of SARS-CoV-2 by a human monoclonal SARS-CoV
664 antibody. *Nature* **583**, 290–295 (2020).

665 23. Ko, S.-Y. *et al.* Enhanced neonatal Fc receptor function improves protection against primate
666 SHIV infection. *Nature* **514**, 642 (2014).

667 24. Zalevsky, J. *et al.* Enhanced antibody half-life improves in vivo activity. *Nat Biotechnol* **28**,
668 157 (2010).

669 25. Gaudinski, M. R. *et al.* Safety and pharmacokinetics of the Fc-modified HIV-1 human
670 monoclonal antibody VRC01LS: A Phase 1 open-label clinical trial in healthy adults. *Plos Med*
671 **15**, e1002493 (2018).

672 26. Bournazos, S., Corti, D., Virgin, H. W. & Ravetch, J. V. Fc-optimized antibodies elicit CD8
673 immunity to viral respiratory infection. *Nature* 1–9 (2020) doi:10.1038/s41586-020-2838-z.

674 27. Weitzenfeld, P., Bournazos, S. & Ravetch, J. V. Antibodies targeting sialyl Lewis A mediate
675 tumor clearance through distinct effector pathways. *J Clin Invest* **129**, 3952–3962 (2019).

676 28. Bournazos, S., Corti, D., Virgin, H. W. & Ravetch, J. V. Fc-optimized antibodies elicit CD8
677 immunity to viral respiratory infection. *Nature* 1–9 (2020) doi:10.1038/s41586-020-2838-z.

678 29. Diamond, M. *et al.* SARS-CoV-2 variants show resistance to neutralization by many
679 monoclonal and serum-derived polyclonal antibodies. *Res Square* (2021) doi:10.21203/rs.3.rs-
680 228079/v1.

681 30. Chen, R. E. *et al.* Resistance of SARS-CoV-2 variants to neutralization by monoclonal and
682 serum-derived polyclonal antibodies. *Nat Med* 1–10 (2021) doi:10.1038/s41591-021-01294-w.

683 31. Kallewaard, N. L. *et al.* Structure and Function Analysis of an Antibody Recognizing All
684 Influenza A Subtypes. *Cell* **166**, 596–608 (2016).

685 32. DiLillo, D. J., Tan, G. S., Palese, P. & Ravetch, J. V. Broadly neutralizing hemagglutinin
686 stalk–specific antibodies require FcγR interactions for protection against influenza virus in vivo.
687 *Nat Med* **20**, 143–151 (2014).

688 33. Dunand, C. J. H. *et al.* Both Neutralizing and Non-Neutralizing Human H7N9 Influenza
689 Vaccine-Induced Monoclonal Antibodies Confer Protection. *Cell Host Microbe* **19**, 800–813
690 (2016).

691 34. Leon, P. E. *et al.* Optimal activation of Fc-mediated effector functions by influenza virus
692 hemagglutinin antibodies requires two points of contact. *Proc National Acad Sci* **113**, E5944–
693 E5951 (2016).

694 35. Bruhns, P. *et al.* Specificity and affinity of human Fcγ receptors and their polymorphic
695 variants for human IgG subclasses. *Blood* **113**, 3716–3725 (2009).

696 36. Weitzenfeld, P., Bournazos, S. & Ravetch, J. V. Antibodies targeting sialyl Lewis A mediate
697 tumor clearance through distinct effector pathways. *J Clin Invest* **129**, 3952–3962 (2019).

698 37. Cheng, Z. J. *et al.* Development of a robust reporter-based ADCC assay with frozen, thaw-
699 and-use cells to measure Fc effector function of therapeutic antibodies. *J Immunol Methods* **414**,
700 69–81 (2014).

701 38. Arvin, A. M. *et al.* A perspective on potential antibody-dependent enhancement of SARS-
702 CoV-2. *Nature* 1–11 (2020) doi:10.1038/s41586-020-2538-8.

703 39. Joyner, M. J. & Wright, R. S. Safety Update: CO VID-19 Convalescent Plasma in
704 20,000 Hospitalized Patients. *Mayo Clinic Proceedings* (2020).

705 40. Arvin, A. M. *et al.* A perspective on potential antibody-dependent enhancement of SARS-
706 CoV-2. *Nature* **584**, 353–363 (2020).

707 41. Khurana, S. *et al.* Vaccine-induced anti-HA2 antibodies promote virus fusion and enhance
708 influenza virus respiratory disease. *Sci Transl Med* **5**, 200ra114 (2013).

709 42. Winarski, K. L. *et al.* Antibody-dependent enhancement of influenza disease promoted by
710 increase in hemagglutinin stem flexibility and virus fusion kinetics. *Proc National Acad Sci* **116**,
711 15194–15199 (2019).

712 43. Hui, K. P. Y. *et al.* Tropism, replication competence, and innate immune responses of the
713 coronavirus SARS-CoV-2 in human respiratory tract and conjunctiva: an analysis in ex-vivo and
714 in-vitro cultures. *Lancet Respir Medicine* (2020) doi:10.1016/s2213-2600(20)30193-4.

715 44. Liu, Z. *et al.* Identification of Common Deletions in the Spike Protein of Severe Acute
716 Respiratory Syndrome Coronavirus 2. *J Virol* **94**, (2020).

717 45. Baum, A. *et al.* Antibody cocktail to SARS-CoV-2 spike protein prevents rapid mutational
718 escape seen with individual antibodies. *Science* **369**, 1014–1018 (2020).

719 46. Thomson, E. C. *et al.* Circulating SARS-CoV-2 spike N439K variants maintain fitness while
720 evading antibody-mediated immunity. *Cell* (2021) doi:10.1016/j.cell.2021.01.037.

721 47. Starr, T. N., Greaney, A. J., Dingens, A. S. & Bloom, J. D. Complete map of SARS-CoV-2
722 RBD mutations that escape the monoclonal antibody LY-CoV555 and its cocktail with LY-
723 CoV016. doi:10.1101/2021.02.17.431683.

724 48. Wise, J. Covid-19: The E484K mutation and the risks it poses. *Bmj* **372**, n359 (2021).

725 49. VIR-7831 for the Early Treatment of COVID-19 in Outpatients - Full Text View -
726 ClinicalTrials.gov. https://clinicaltrials.gov/ct2/show/NCT04545060?term=VIR-
727 7831&draw=2&rank=2.

728 50. A Study of Immune System Proteins in Participants With Mild to Moderate COVID-19
729 Illness - Full Text View - ClinicalTrials.gov.
730 https://clinicaltrials.gov/ct2/show/NCT04634409?term=VIR-7831&draw=2&rank=3.

731 51. Vir Biotechnology and GSK announce NHS-supported AGILE study to evaluate VIR-7832
732 in the early treatment of COVID-19 | GSK. *undefined* https://www.gsk.com/en-gb/media/press-
733 releases/vir-biotechnology-and-gsk-announce-nhs-supported-agile-study-to-evaluate-vir-7832-
734 in-the-early-treatment-of-covid-19/.

735 52. Wise, J. Covid-19: New coronavirus variant is identified in UK. *Bmj* **371**, m4857 (2020).

736 53. CoVariants. https://covariants.org/.

737 54. Piccoli, L. *et al.* Mapping neutralizing and immunodominant sites on the SARS-CoV-2 spike
738 receptor-binding domain by structure-guided high-resolution serology. *Cell* (2020)
739 doi:10.1016/j.cell.2020.09.037.

740 55. Rappazzo, C. G. *et al.* Broad and potent activity against SARS-like viruses by an engineered
741 human monoclonal antibody. *Science* **371**, 823–829 (2021).

742 56. Sette, A. & Crotty, S. Adaptive immunity to SARS-CoV-2 and COVID-19. *Cell* **184**, 861–
743 880 (2021).

744 57. Stettler, K. *et al.* Specificity, cross-reactivity and function of antibodies elicited by Zika virus
745 infection. *Science* **353**, aaf8505 (2016).

746

747 **FIGURE LEGENDS**

748 **Figure 1.** VIR-7831 and VIR-7831 bind S and neutralize SARS-CoV-2 virus and S variants of concern in
749 vitro. a) Binding of VIR-7831 (black circles) and VIR-7832 (blue squares) to SARS-CoV-2 RBD was
750 tested by ELISA. Shown is the average of four replicates and SD derived from three independent
751 experiments. b) Association and dissociation profiles of VIR-7831 to SARS-CoV-2-RBD were measured
752 using SPR. The double reference subtracted curves (shown for single replicates) are plotted together with
753 the curve fit in black (obscured by close overlay with the data). Values are from two independent
754 experiments. c) Binding of VIR-7831 (black circles) and VIR-7832 (blue squares) to cell-surface S
755 protein was determined by flow cytometry. Data are expressed as the percentage of the positive cells.
756 Results shown are from one experiment and representative of three independent experiments performed.
757 d) In vitro neutralization of live SARS-CoV-2 by different concentrations of VIR-7831 (left) and VIR-
758 7832 (right) measured by nucleocapsid staining 6-hours post-infection. Results shown are from one
759 experiment and representative of at least two independent experiments performed.

760 **Figure 2.** VIR-7831 and VIR-7832 demonstrate effector function in vitro. In vitro effector function (a-e)
761 activation profiles of human FcγRIIa (a), FcγRIIb (b), FcγRIIIa low-affinity (F158) (c) or FcγRIIIa high-
762 affinity binding allele (V158) (d) using bioreporter assays using S-expressing CHO cells as the target

763 antigen. Data points show means± SD of duplicates. NK-cell mediated killing (ADCC) of S-expressing
764 CHO cells using freshly isolated cells from two donors previously genotyped for homozygous expression
765 of low-affinity (F/F158) (e) or high-affinity (V/V158) FcγRIIIa (f). Data points are means of
766 quadruplicates ± SD. g) Antibody-dependent cellular phagocytosis (ADCP) using S-expressing CHO cells
767 and freshly isolated PBMCs. Data represent the means of duplicates ± SD.

768 **Figure 3.** VIR-7831 shows in vivo efficacy in a hamster SARS-CoV-2 model of infection. a) Overview
769 of hamster in vivo study design. b) and c) Animal weight over time as a percent of starting weight in
770 animals dosed a Day -1 (b) or Day -2 (c). Medians of at least N=6 animals and interquartile range are
771 shown. d) and e) Day 4 terminal weights expressed as a percentage of starting weight for animals dosed at
772 Day -1 (d) or Day -2 (e). Bar denotes median values. f) and g) Day 4 lung viral load in Day -1 (f) or Day -
773 2 (g) treated animals as assessed by RT-qPCR. Bar denotes median values. h) and i) infectious virus in
774 lung at Day 4 for Day -1 (h) or Day -2 (i) dosed animals. Bar denotes median values. ns=not significant,
775 ** = $p<0.05$, and *** = <0.005 as assessed by the Mann-Whitney U-test.

776 **Table 1.** VIR-7831 and VIR-7832 retain activity against S variants of concern in an authentic virus
777 system**.** Average fold change in VIR-7831 and VIR-7832 IC_{50} compared to relative wild-type controls for
778 S variants tested in an authentic virus system. Data shown are averages of at least two independent
779 experiments.

780 **Table 2.** VIR-7831 and VIR-7832 retain activity against S variants of concern in a pseudotyped virus
781 system**.** Average fold change in VIR-7831 and VIR-7832 IC_{50} compared to relative wild-type controls for
782 S variants tested in a VSV/VeroE6 pseudotyped virus system. Data shown are averages of at least two
783 independent experiments.

784 **Table 3.** VIR-7831 and VIR-7832 retain activity against variants that confer resistance to authorized
785 mAbs. Activity of VIR-7831 against variants conferring reduced susceptibility to bamlanivimab,
786 imdevimab or casirivimab in a VSV/VeroE6 pseudotyped virus system. The geometric mean of IC_{50}s and

787 average fold-change versus the relative wild-type control from at least two independent experiments are
788 shown.

789 **Table 4.** The VIR-7831/VIR-7832 epitope is highly conserved. Conservation data comprising >1,700,000
790 sequences from the GISAID database and variants at each position are shown. Variants in bold were
791 tested in a pseudotyped virus assay.

792 **Table 5.** Activity of VIR-7831 against epitope variants. VIR-7831/VIR-7832 epitope variants detected in
793 sequences from the GISAID database were tested in a VSV/VeroE6 pseudotyped virus system. The
794 geometric mean of IC_{50}s and average fold-change versus the relative wild-type control from at least two
795 independent experiments are shown. Variants marked with "a" indicates that the data shown are from the
796 parental antibody S309.

797 **Supplemental Figure 1.** Binding of VIR-7831 and VIR-7832 to human FcγRs and C1q as measured by
798 SPR. Binding of VIR-7831 and VIR-7832 to a) human FcγRIIa (H131 and R131 alleles), FcγRIIIa (F158
799 and V158 alleles) and FcγRIIb were measured using SPR. Biotinylated purified FcγRs were captured on
800 the sensor chip surface prior to injection of VIR-7831 or VIR-7832. Association and dissociation profiles
801 (separated by the vertical dotted line) were measured in real time as change in the SPR signal. b) Binding
802 of VIR-7831 and VIR-7832 to complement component C1q was measured using BLI on an Octet Red96
803 instrument. Association and dissociation profiles (separated by the vertical dotted line) were measured in
804 real time as change in the interference pattern.

805 **Supplemental Figure 2.** Sub-neutralizing concentrations of VIR-7831 and VIR-7832 do not enhance
806 viral entry, viral replication or cytokine production in vitro. Internalization (a) and replication (b) of
807 SARS-CoV-2 was evaluated in VeroE6, moDCs or PBMCs at various timepoints. Two independent
808 experiments with human moDCs and PBMCs from three individual donors were analyzed (5 unique
809 moDC donors, 6 unique PBMC donors total between two experiments). VeroE6 cells were run in
810 duplicate for both independent experiments. Data from each replicate well from two independent

811 experiments are plotted as individual points, with horizontal lines representing the median. Mann-
812 Whitney U-test comparison to no antibody group, *$p<0.05$. c) Supernatant cytokine and chemokine levels
813 as measured by MSD at the indicated time post infection. Data from two independent experiments (three
814 replicates each, five unique donors) are plotted as the mean and SD.

815 **Supplemental Figure 3.** Overview of VIR-7832 resistance selection method. All passaging was
816 conducted in duplicate wells. (a) VIR-7832 concentration was increased during each passage. P3 X
817 indicates passage 3 virus, after which virus was lost with subsequent increases in concentration. In (b) and
818 (c), p3X denotes where passage 3 virus from (a) was used to initiate (b) viral lineage 1 and (c) viral
819 lineage 2. Arrows indicate passages that were subjected to sequence analysis, and * indicate the passages
820 in lineage 1 with no detectable virus or CPE. Selection continued for a total of eight passages.

821 **Supplemental Table 1.** Amino acid substitutions identified in the SARS-CoV-2 S upon in vitro selection
822 with VIR-7832. Spike gene sequences were compared to a SARS-CoV-2 reference sequence (NCBI:
823 NC_045512.2) to identify variants. Fold-changes in IC_{50} were determined compared to the SARS-CoV-2
824 virus stock.

825 **Supplemental Table 2.** VIR-7831 and VIR-7832 activity against selected S variants. VIR-7831/VIR-
826 7832 epitope variants observed by in vitro resistance selection were individually tested in a VSV/VeroE6
827 pseudotyped virus system. The geometric mean of IC_{50}s and average fold-change versus the relative wild-
828 type control from at least two independent experiments are shown.

829

Figure 1

a)

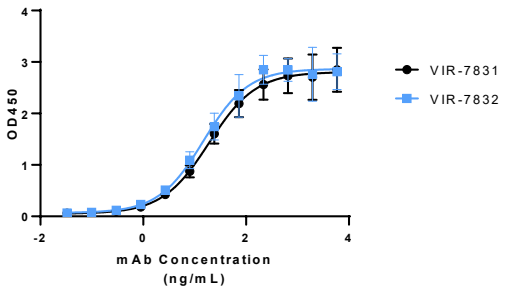

b)

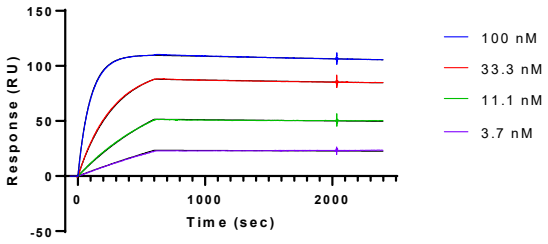

c)

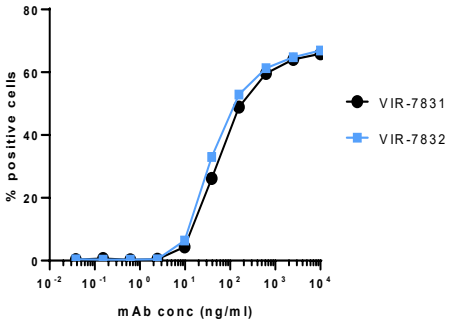

d)

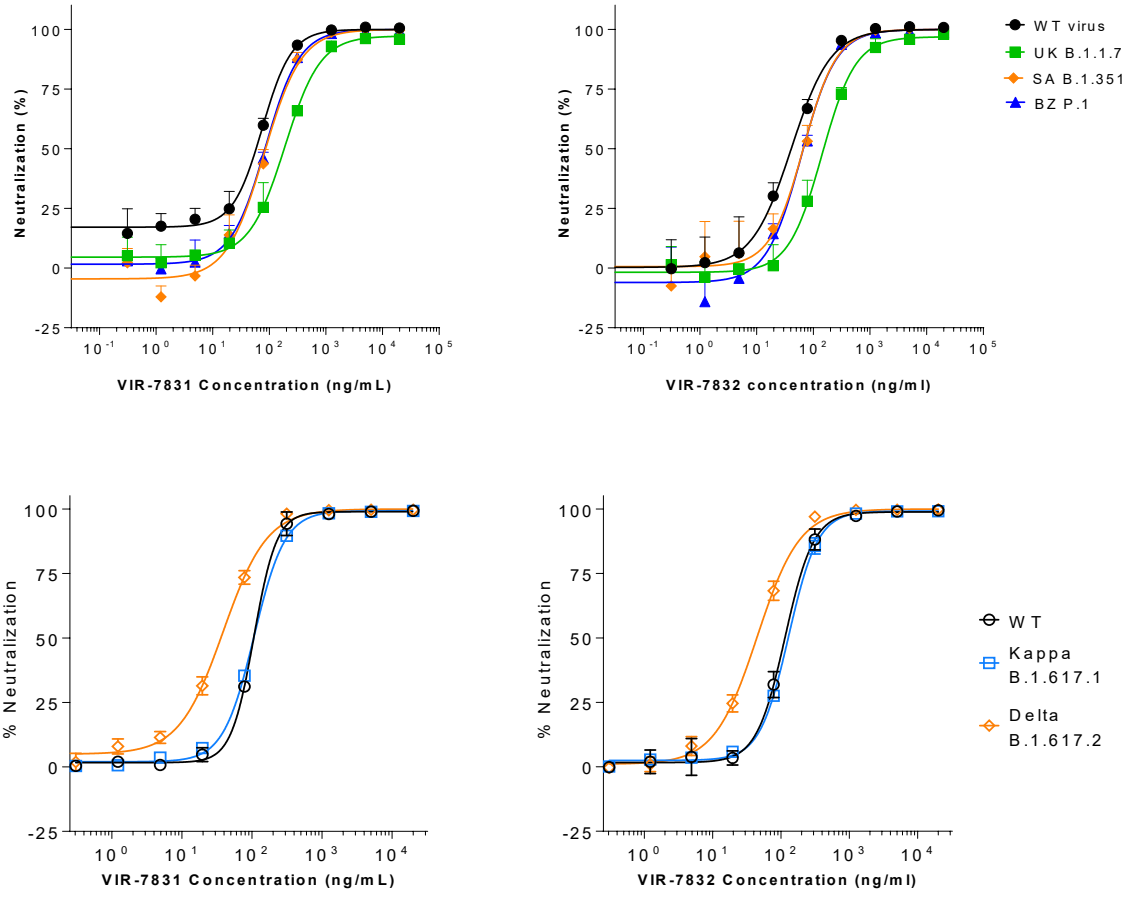

Figure 2

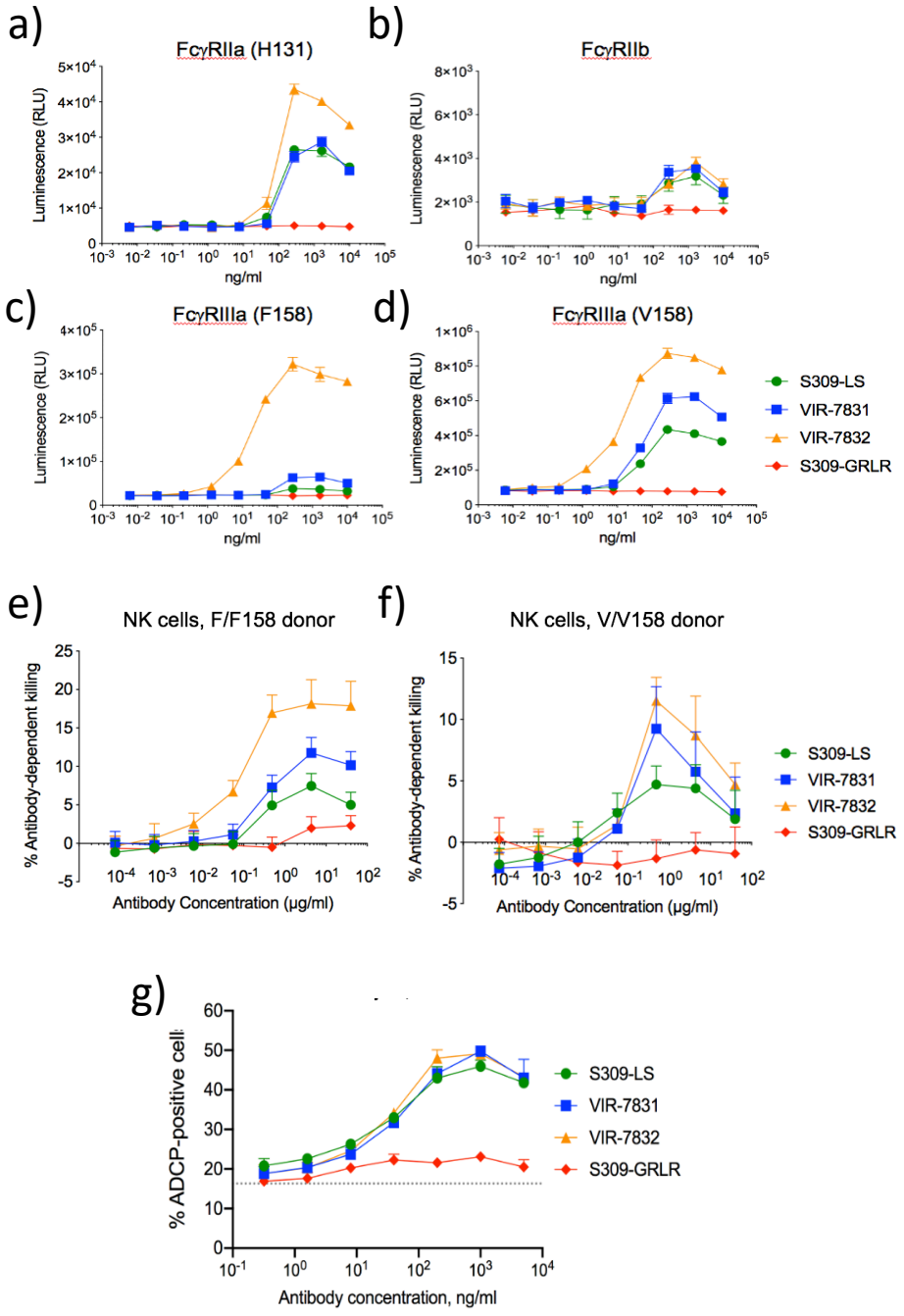
a)
FcγRIIa (H131)
Luminescence (RLU)
ng/ml
b)
FcγRIIb
Luminescence (RLU)
ng/ml
c)
FcγRIIIa (F158)
Luminescence (RLU)
ng/ml
d)
FcγRIIIa (V158)
Luminescence (RLU)
ng/ml
S309-LS
VIR-7831
VIR-7832
S309-GRLR
e)
NK cells, F/F158 donor
% Antibody-dependent killing
Antibody Concentration (μg/ml)
f)
NK cells, V/V158 donor
% Antibody-dependent killing
Antibody Concentration (μg/ml)
S309-LS
VIR-7831
VIR-7832
S309-GRLR
g)
% ADCP-positive cell
Antibody concentration, ng/ml
S309-LS
VIR-7831
VIR-7832
S309-GRLR

Figure 3

a)

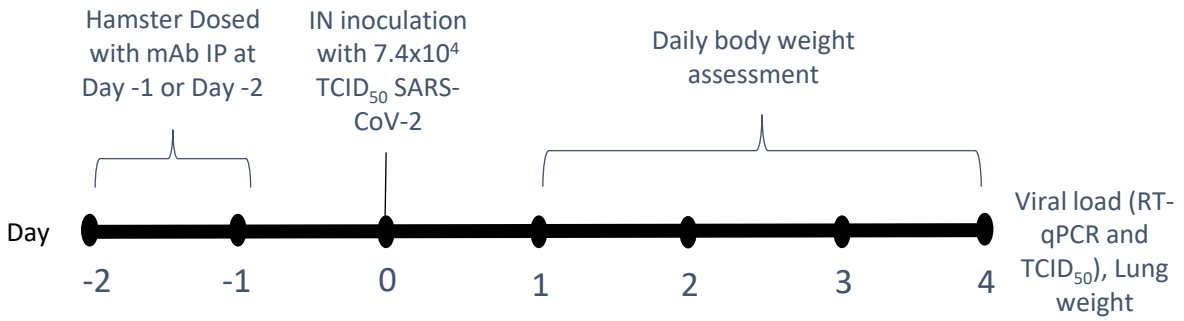

b)

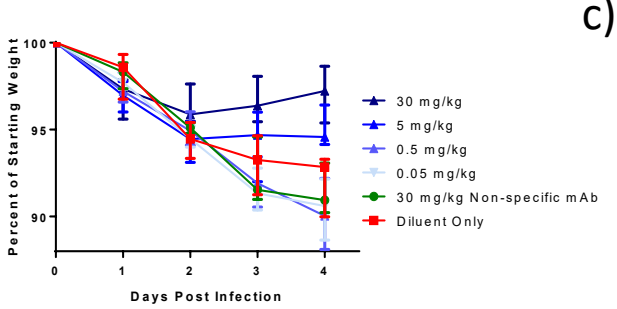

c)

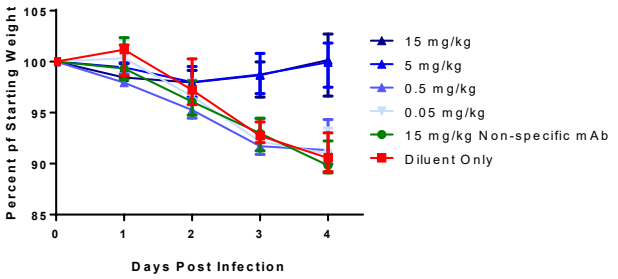

d)

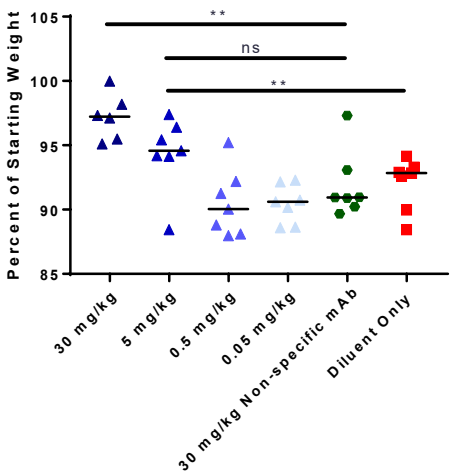

e)

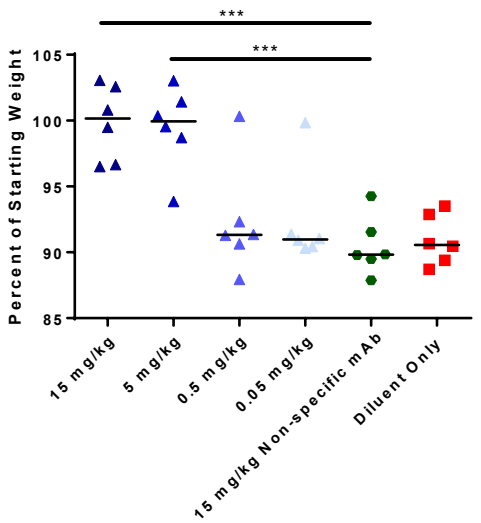

f)

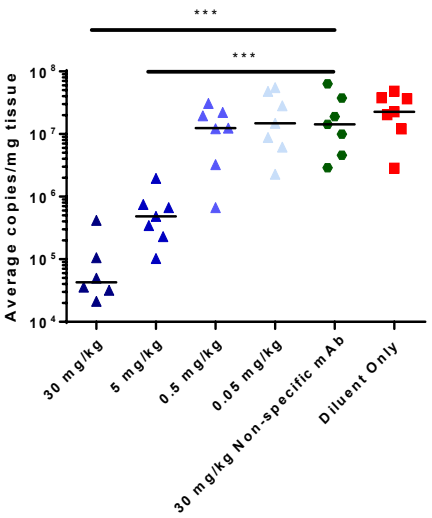

g)

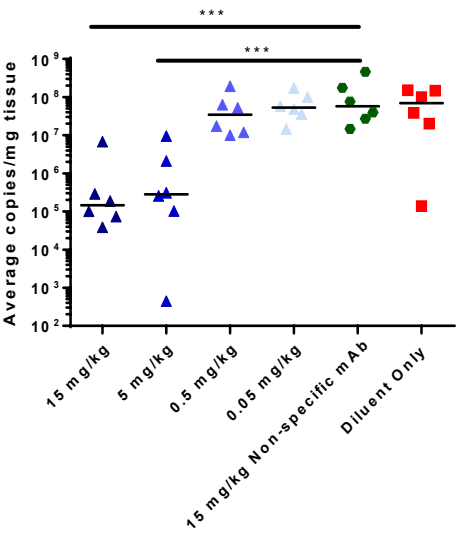

h)

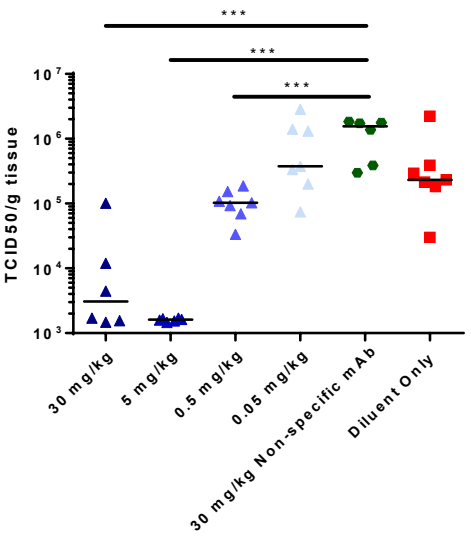

i)

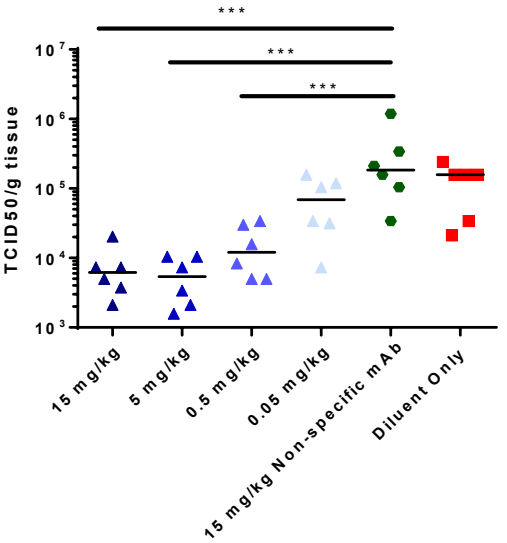

Table 1

SARS-CoV-2 Variant	**Geometric Mean VIR-7831 IC_{50} (ng/ml) (Average Fold Change IC_{50} vs. Wild-Type)**	**Geometric Mean VIR-7831 IC_{90} (ng/ml) (Average Fold Change IC_{90} vs. Wild-Type)**	**Geometric Mean VIR-7832 IC_{50} (ng/ml) (Average Fold Change IC_{50} vs. Wild-Type)**	**Geometric Mean VIR-7832 IC_{90} (ng/ml) (Average Fold Change IC_{90} vs. Wild-Type)**
Alpha (B.1.1.7)	187.15 (3.0)	1246.86 (4.1)	181.12 (3.1)	1222.95 (3.7)
Beta (B.1.351)	71.89 (1.2)	385.01 (1.3)	59.67 (1.1)	309.84 (0.9)
Gamma (P.1)	73.11 (1.6)	335.79 (1.4)	48.94 (1.2)	217.02 (0.9)
Delta (B.1.617.2)	118.64 (0.9)	379.89 (1.0)	132.37 (1.0)	428.83 (1.0)
Kappa (B.1.617.1)	51.29 (0.4)	219.08 (0.6)	59.13 (0.5)	274.24 (0.7)

Table 2

Variant	**Spike Mutations**	**Fold-Change in VIR-7831 IC_{50} vs. Wild-type**	**Fold-Change in VIR-7832 IC_{50} vs. Wild-type**
Alpha (B.1.1.7)	H69-, V70-, Y144-, N501Y, A570D, D614G, P681H, T716I, S982A, D1118H	2.3	2.5
Beta (B.1.351)	L18F, D80A, D215G, R246I, K417N, E484K, N501Y, D614G, A701V	0.6	0.7
Gamma (P.1)	D138Y, D614G, E484K, H655Y, K417T, L18F, N501Y, P26S, R190S, T1027I, T20N, V1176F	0.4	0.4
Delta (B.1.617.2)	T19R, G142D, E156G, F157-, R158-, L452R, T478K, D614G, P681R, D950N	1	NT
Epsilon (B.1.427/B.1.429)	S13I, W152C, L452R, D614G	0.7	NT
Eta (B.1.525)	Q52R, A67V, H69-, V70-, Y144-, E484K, D614G, Q677H, F888L	0.9	NT
Iota (B.1.526)	L5F, T95I, D253G, E484K, D614G, A701V	0.6	NT
Kappa (B.1.617.1)	T95I, G142D, E154K, L452R, E484Q, D614G, P681R, Q1071H	0.7	NT
Lambda (C.37)	G75V, T76I, del246-252, L452Q, F490S, T859N	1.5	NT
Delta Plus (AY.1)	T19R, T95I, G142D, E156G, F157-, R158-, W258L, K417N, L452R, T478K, D614G, P681R, D950N	1.1	NT
Delta Plus (AY.2)	T19R, V70F, G142D, E156G, F157-, R158-, A222V, K417N, L452R, T478K, D614G, P681R, D950N	1.3	NT
Mexico/Swiss (B.1.1.519)	T478K, D614G, P681H, T732A	0.8	NT
Scotland (B.1.258)	H69-, V70-, N439K, D614G	0.9	NT
US (R.2)	E484K, D614G, Q677H, T732S, E1202Q	0.8	NT
Liverpool (A.23.1)	R102I, F157L, V367F, E484K, Q613H, P681R	1.1	NT
Cameroon (B.1.619)	I210T, N440K, E484K, D614G, D936N, S939F, T1027I	1.3	NT
Bristol (B.1.1.7+E484K)	H69-, V70-, Y144-, E484K, N501Y, A570D, D614G, P681H, T716I, S982A, D1118H	1.7	NT
Mu (B.1.621)	T95I, Y144T, Y145S, ins146N, R346K, E484K, N501Y, D614G, P681H, D950N	1.3	NT

Table 3

Amino Acid position	Substitution / Deletion	mAb with Reduced Susceptibility	Variants in Tested Spike Sequence	VIR-7831 EC_{50} (ng/ml)	Average Fold Change in EC_{50} Compared to Relative Wild-Type
E406	W	casirivimab+ imdevimab	E406W	53.66	0.74
K417	E	casirivimab	K417E	67.71	0.89
N439	K	imdevimab	N439K, D614G	17.05	0.86
N440	D	imdevimab	N440D	80.47	1.29
N440	K	imdevimab	N440K, D614G	19.99	0.48
K444	Q	imdevimab	K444Q	79.68	1.11
V445	A	imdevimab	V445A	41.74	3.38
G446	V/I	imdevimab	G446V, D614G	18.41	1.50
Y453	F	casirivimab	G261D, Y453F	27.28	2.19
L455	F	casirivimab	L455F, D614G	21.65	0.56
G476	S	casirivimab	G476S	36.97	2.94
E484	K	bamlanivimab	E484K, D614G	12.91	0.33
F486	V/I	casirivimab	F486V	82.24	1.10
Y489	H	casirivimab	Y489H	92.29	1.48
F490	S	bamlanivimab	F490S	33.10	0.85
Q493	K	casirivimab, bamlanivimab	Q483K	69.79	0.98
S494	P	casirivimab, bamlanivimab	S494P, D614G	29.10	2.50

Table 4

Amino Acid Position	Reference Amino Acid[a]	Variants Identified in order of Prevalence[b]	Percent Reference AA Conservation
332	I	**V, T**	>99.99
333	T	**I**, K, A	>99.99
334	N	**Y**, **K, H**, S, D, T	>99.99
335	L	**F**, **S**, V, M	99.99
336	C	S	>99.99
337	P	**S**, **T**, **L**, **H**, **R**, K	>99.99
339	G	**D**, **S, V**, **C**, F, N	99.98
340	E	D, **K, G**, **A, Q**	>99.99
341	V	**I**, A, F, P, S	>99.99
343	N	Y, K, **S**	>99.99
344	A	**S**, **V**, **T**, D, F, P	99.98
345	T	**S**, I, **N**	>99.99
346	R	**S**, **K**, **I**, **T**, **G**, F	99.89
354	N	**K**, **D**, **S**, **H**, **I**, T, Y, G	99.96
356	K	**R, M**, **N**, **T**, E, G, Q, W, Y, I	99.99
357	R	**K, I**, G, T, C, L	99.93
358	I	**V**, T, **F**, **L**, A, E	>99.99
359	S	**T**, **N**, **G**, **R**, C, F, I	99.98
360	N	**Y**, S, F, A, L, T	>99.99
361	C	T, G, F, R, N, S	>99.99
440	N	**K**, **S**, **Y**, **T**, **D**, I, H, F, R	99.83
441	L	**R**, **F**, **I**, **V**, Y, H, M, S, E, N	>99.99
509	R	K, T, I, S	>99.99

Table 5

Epitope Reference Amino Acid	Amino Acid Changes in Spike protein	Geomean Neutralization EC_{50} (ng/mL)	Average Fold-Change EC_{50} Relative to Wild-Type
I332	I332V, D614G	53.43	1.48
	I332T, D614G	66.74	1.61
N334	N334H, D614G	30.74	0.87
	N334Y, D614G	32.89	0.96
L335	L335S, D614G	29.80	0.85
P337	P337L, D614G	>10000	>192
	P337H, D614G	185.29	5.13
	P337T, D614G	383.27	10.62
	P337R, D614G	>10000	>192
G339	G339V, D614G	78.32	1.26
E340	E340Q, D614G	>2500	>50
	E340G, D614G	640.07	18.21
N343	N343S, D614G	16.87	0.48
A344	A344V, D614G	53.87	1.14
T345	T345S, D614G	42.92	0.69
	T345N, D614G	20.29	0.57
R346	R346G, D614G	43.73	0.85
N354	N354I, D614G	37.09	1.05
K356	K356M, D614G	64.09	1.03
	K356T, D614G	281.13	5.90
I358	I358F, D614G	42.69	1.19
S359	S359T, D614G	39.98	0.84
N360	N360S, D614G	34.08	0.72
	N360Y, D614G	29.67	0.61
N440	N440T, D614G	50.81	0.82
L441	L441R, D614G	42.30	0.87
	L441V, D614G	48.24	0.98

Supplemental Figure 1

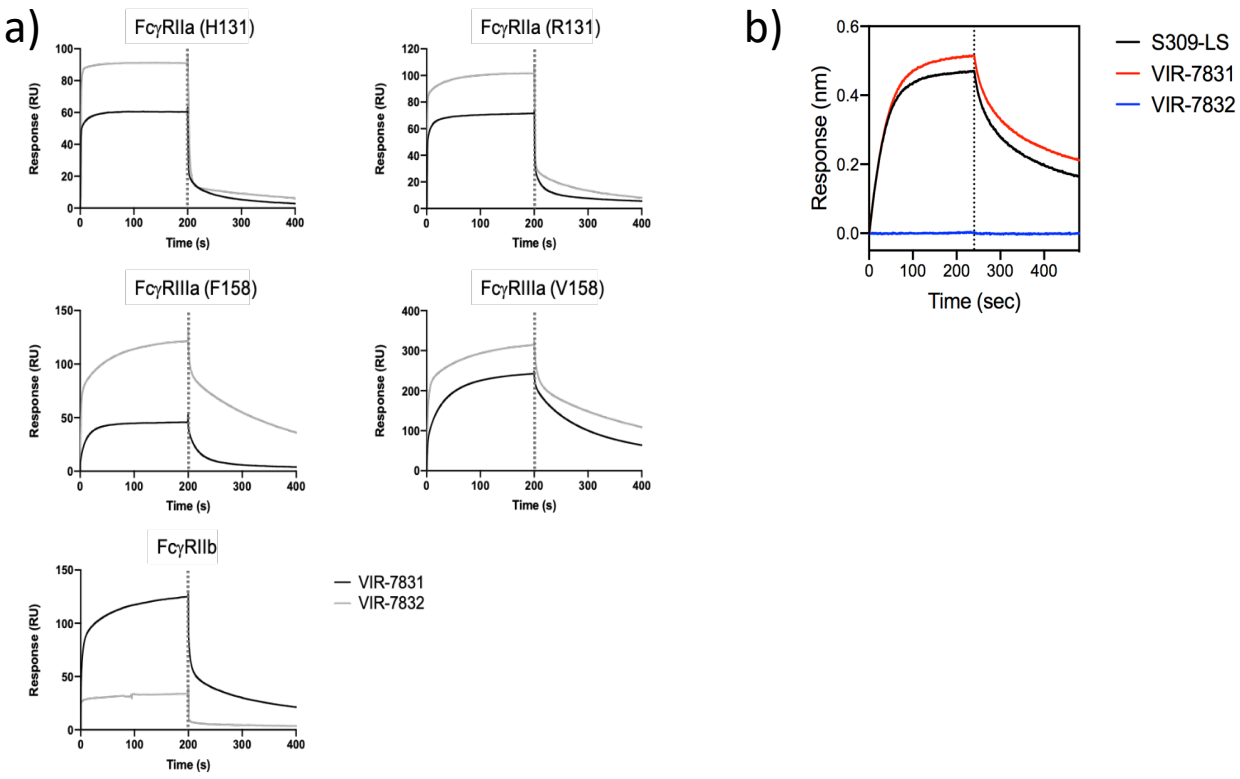

Supplemental Figure 2

a)

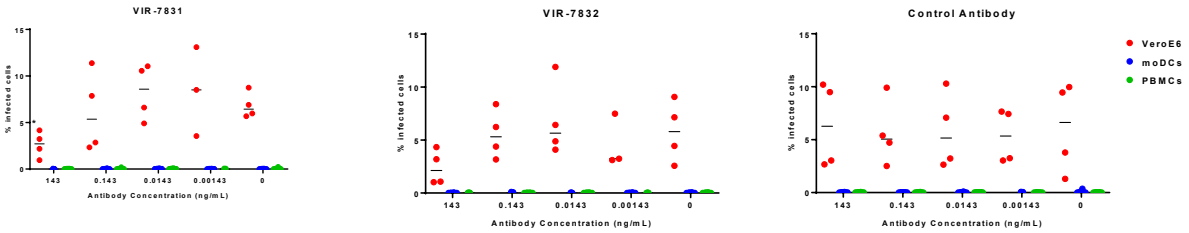

b)

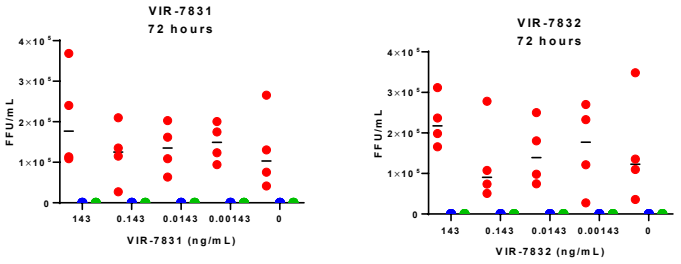

c)

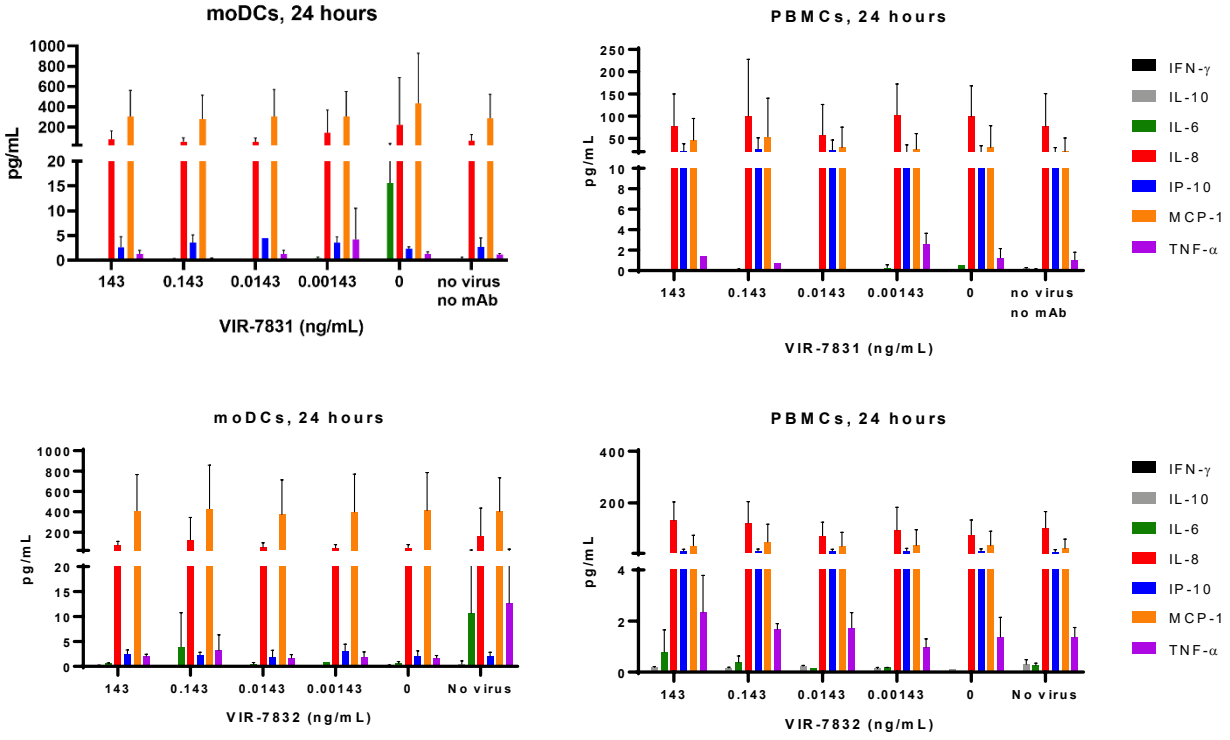

Supplemental Figure 3

a)

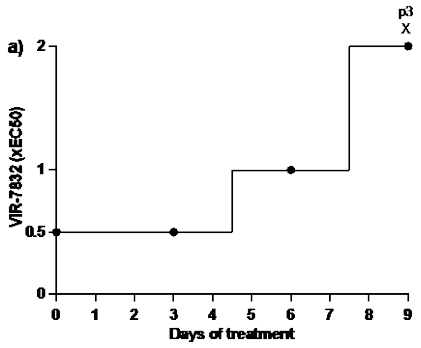

b)

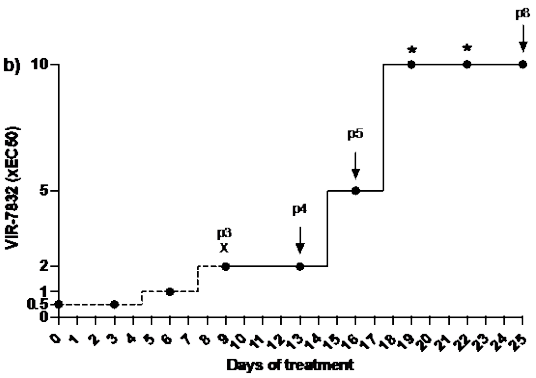

c)

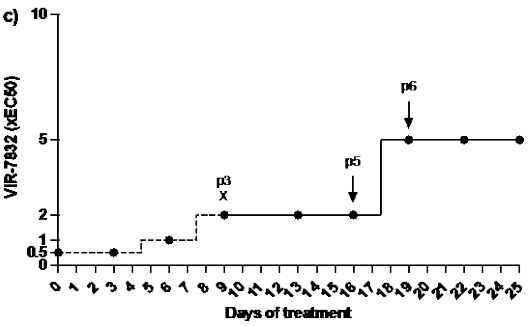

Supplemental Table 1

Passage	**Spike Gene Amino Acid Substitution (Freq)** [a,b]	**EC_{50} (µg/mL)**	**Fold Change in EC_{50} to WT**[c]
SARS-CoV-2 virus stock[c]	H66R (5.7%) N74K (12.6%) T76I (5.6%) 215-216insKLRS (60.9%) H655Y (3.1%)	0.06	NA
VIR-7832 Lineage 1, passage 4	215-216insKLRS (74.5%) 675-679 del (20.6%)	0.34	5.64
VIR-7832 Lineage 1, passage 5	215-216insKLRS (74.6%) 675-679del (66.0%)	0.35	5.93
VIR-7832 Lineage 1, passage 8	215-216insKLRS (74.7%) E340A (98.7%) 675-679del (84.5%)	ND	>10
VIR-7832 Lineage 2, passage 5	215-216insKLRS (73.9%) 675-679del (47.3%) R682W (4.9%) V1128F (3.5%)	0.32	5.40
VIR-7832 Lineage 2, passage 6	215-216insKLRS (75.3%) 675-679del (74.2%) R682W (4.9%) V1128F (30.9%)	0.39	6.54

Supplemental Table 2

Amino Acid Changes in Spike protein	VIR-7831		VIR-7832	
	Geomean Neutralization EC_{50} (ng/mL)	Fold Change Relative to Wild-Type	Geomean Neutralization EC_{50} (ng/mL)	Fold Change Relative to Wild-Type
Wild Type[a]	104.46	NA	100.75	NA
E340A	> 10,000	>100	> 10,000	> 107
R682W	53.96	0.52	47.78	0.49
V1128F	50.65	0.53	49.69	0.60